Nanoscale Advances

REVIEW

View Article Online
View Journal | View Issue

Cite this: *Nanoscale Adv.*, 2025, **7**, 1243

Structure–activity relationships in the development of single atom catalysts for sustainable organic transformations

Deepshikha Roy and Kalyanjyoti Deori *

Single atom catalysts (SACs), which can provide the combined benefits of homogeneous and heterogeneous catalysts, are a revolutionary concept in the field of material research. The highly exposed catalytic surfaces, unsaturated sites, as well as unique structural and electronic properties of SACs have the potential to catalyze numerous reactions with unmatched efficiency and durability when stabilized on a suitable support. In this review, we have provided an intuitive insight into the strategies adopted in the last 5 years for morphology control of SACs to know about its impact on metal–support interaction and various organic transformations with special reference to metal oxides, alloys, metal–organic frameworks (MOFs) and carbon-based supports. This review also includes a brief description of unparalleled potentials of SACs and the recent advances in the catalysis of industrially important organic transformations, with special emphasis on the C–C cross-coupling reaction, biomass conversion, hydrogenation, oxidation and click chemistry. This unprecedented and unique perspective will highlight the interactions occurring within SACs that are responsible for their high catalytic efficiency, which will potentially benefit various organic transformations. We have also suggested plausible synergy of various other concepts such as defect engineering and piezocatalysis with SACs, which can provide a new direction to sustainable chemistry. A good understanding of the different types of metal–support interactions will help researchers develop morphology-controlled SACs with tunable properties and establish mechanisms for their exceptional catalytic behaviour in industrially important organic transformations.

Received 25th May 2024
Accepted 15th January 2025

DOI: 10.1039/d4na00433g

rsc.li/nanoscale-advances

KD's NAME (NanoMat&Energy) Lab, Department of Chemistry, Dibrugarh University, Dibrugarh 786004, India. E-mail: kalchemdu@gmail.com; kalchemdu@dibru.ac.in

Deepshikha Roy

Deepshikha Roy is currently pursuing a PhD under the supervision of Dr Kalyanjyoti Deori at the Department of Chemistry of Dibrugarh University, Assam, India. She is a DST-INSPIRE Fellow and her research interest focuses on the development of atomically dispersed catalysts for electrocatalytic applications and sustainable organic transformations. She completed her BSc in Chemistry from D. H. S. K. College and she is a recipient of the University Gold Medal for her MSc in Chemistry from Dibrugarh University.

Kalyanjyoti Deori

Dr Kalyanjyoti Deori, Assistant Professor at Dibrugarh University, received his MSc degree and PhD in Chemistry from the University of Delhi, India, and before joining this University in 2018, he was an Assistant Professor at Kirori Mal College, University of Delhi. He has an extensive publication record in high-impact journals. His research focuses on the development of advanced functional nanomaterials for catalytic applications, leading several funded projects. Dr Deori has received numerous awards, including research fellowships and multiple best poster and paper awards. His work continues to inspire and advance the field of sustainable chemistry and environmental applications.

1. Introduction

The growing energy crisis and depleting resources require a more holistic and sustainable approach for industrially important reactions. The development of atomically dispersed metal catalysts (ADMCs) and single atom catalysts (SACs) for electrocatalytic and photocatalytic reactions is highly sought after in sustainable chemistry. Industrially important organic transformations such as C–C cross coupling and azide–alkyne cycloaddition reactions are important for the production of chemicals, biopolymers, and a variety of pharmaceutical products.[1–8] Lignin and its derivatives used for biomass conversions constitute 15–35% of lignocellulosic biomass by weight, which is extremely crucial for energy and fuel production.[9] However, most organic transformations require harsh reaction conditions and suffer from low atom utilization, poor catalyst recyclability, high cost and complicated procedures.[4,5] Currently, the inevitable use of fossil fuels and the resulting global warming have led the world towards exploration of new renewable resources.

For ages, numerous researchers have been working on a variety of homogeneous and heterogeneous catalysts for a wide range of applications. However, each of these catalysts has its own set of advantages and disadvantages. Homogeneous catalysts often exhibit higher catalytic activity and selectivity, but their high cost and poor recyclability often prove to be disadvantageous in terms of their practical utility. Heterogeneous catalysts are often associated with disadvantages such as poor catalytic efficiency and selectivity but showcase better recyclability, resulting in a cost-effective alternative.[10–12] However, the emergence of SACs with huge potential has led the entire research community to rethink ways and explore the enormous possibilities for developing a catalyst that operates at the fine line between homogeneous and heterogeneous catalysis. ADMCs are the umbrella which fits in the SACs underneath. When the metal atoms exist as dimers, trimers or small clusters of 2–4 atoms on the surface of the support, they are considered to be ADMCs; on the other hand, when the metal atoms remain in complete isolation on the surface of the catalyst, showcasing better structure and catalytically active sites, they fall under the category of SACs. Unlike ADMCs with metal–metal bonds between similar metal atoms, SACs consist of a higher number of unsaturated sites and provide a more tunable local environment, leading to higher activity at an extremely low metal content. Moreover, the catalytically active sites are much more uniform in the case of SACs than ADMCs, resulting in more consistent activity over a longer period.[11,13] The metal atoms are often anchored onto the surface of the support through various vacancies, defects or groups like O^{2-}, S^{2-} *etc.*[11,14] Doped metal catalysts can also be considered as SACs provided there are no metal–metal bonds between similar metal atoms. SACs are excellent electro-photocatalysts with benefits like 100% atom utilization, unsaturated coordination sites, high catalytic efficiency, excellent recyclability, increased interfacial sites and a cost-effective solution.[15–17] However, the high surface energy and poor thermal stability of the SACs limit their application by causing migration and agglomeration during the chemical reactions. So, various semiconducting supports like g-C_3N_4, binary alloys, graphene oxide, doped materials, fullerene, metal–organic frameworks (MOFs) and metal oxides have been proven to significantly enhance stability as well as catalytic activity and selectivity by providing a greater surface area with more catalytically active sites.[16,18]

The development of highly stable SACs will lead us to a more environmentally benign approach involving even natural sunlight to initiate organic reactions in a cost-effective manner. The synergy of highly unsaturated sites with the insertion of new electronic states near the fermi levels of the semiconductors, as shown in Fig. 1, results in an electron pumping system in SACs, which not only enhances the number of catalytically active sites but also narrows down the bandgap of the original semiconducting material so that most of the charges reach the catalyst surface for catalyzing the reaction. Moreover, the homogeneous distribution of single atoms into the lattice matrix and the surface of the support resembles a molecular

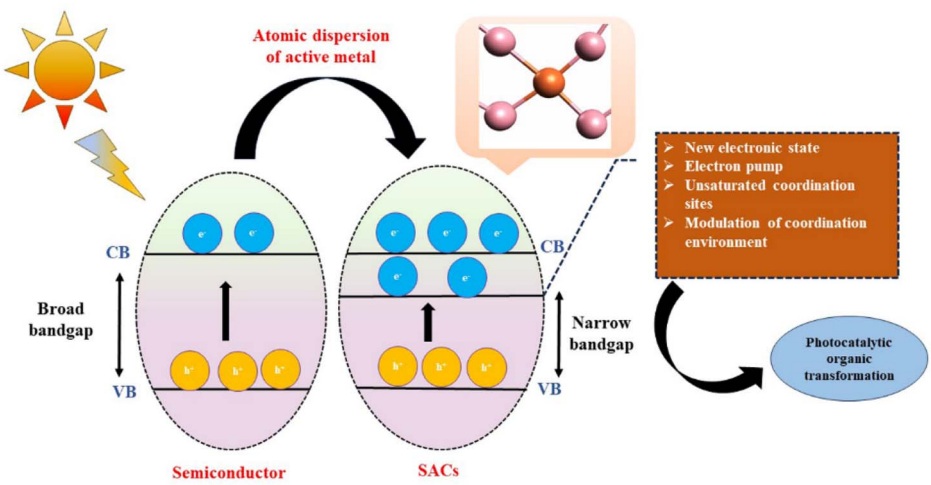

Fig. 1 A depiction of bandgap modulation through the development of SACs.

complex suitable for organic reactions usually catalyzed by homogeneous catalysts.[19,20] It has also been observed that the precise control over the morphology of the supports, along with modulation of the local environment of the single atom, can also help in enhancing the stability of the catalyst as well as lowering the activation energy of the substrates by deciding their coordination modes during the reaction.[21] So, this review briefly summarizes the recent advances in the last five years in the field of SACs for industrially important organic transformations with special emphasis on the C–C cross coupling reaction, biomass conversion, hydrogenation, oxidation and click chemistry. A fresh perspective is provided in this review for uniting various works together to highlight the versatility of SACs. This review puts the limelight on the multifunctionality of SACs for various organic reactions, which can be achieved by their structure and morphology modulation. Most of the literature so far has explained the fundamentals of SACs and their applications. Very few works provide the structure–activity relations for such organic reactions. However, there is still much to know about their unique bandgap properties and the morphological impact of SACs in catalysis. This review also attempts to establish the morphology–activity relations of SACs for their utmost efficiency so that such a morphology-controlled strategy can also be utilized for catalyzing organic reactions. The exposed planes of SACs have the potential to guide the researchers not only to make the process of SAC development and catalysis hassle-free but also to enhance the loading of the isolated active centers for their practical application. Instead of just focusing on the efficiency of the SACs and reiterating already published works, this review tries to establish a relationship between various works and highlight new concepts like defect engineering and piezocatalysis for SAC development, which can prove to be an engrossing field in the near future. This review provides a comprehensive summary of the recent strategies used for the development of highly stable SACs and tries to put forward plausible reasons behind their high selectivity for specific organic reactions.

2. Strategies and the impact of morphology control and metal–support interactions on the stability and efficiency of SACs

SACs can be both supported as well as unsupported. Providing support with a large surface area to anchor the isolated metal atoms increases the durability of the catalysts. However, developing highly stable unsupported SACs like single atom alloy (SAA) is considered to be even better as it increases the cost-effectiveness of the process without compromising its catalytic efficiency. Each of the supported and unsupported SACs has its own set of advantages as well as disadvantages. Thus, it becomes extremely crucial to understand various metal–supports and metal–metal interactions in both types of SACs to develop more chemoselective catalysts. Moreover, the modulation of morphology and coordination environment of the SACs also affect their stability.[20–29] So, this section summarizes the different strategies that can be used for the modulation of metal–support interactions to enhance their stability, activity as well as selectivity for various reactions.

2.1 Supported SACs

The kind of support used for the development of SACs plays a crucial role in deciding the efficiency and selectivity of the catalyst, as a strong metal–support interaction can induce a change in the electronic structure and geometry of the metals and support, resulting in better atomic dispersion.[20] Supports with high surface area to volume ratios like metal oxides,[22,23]

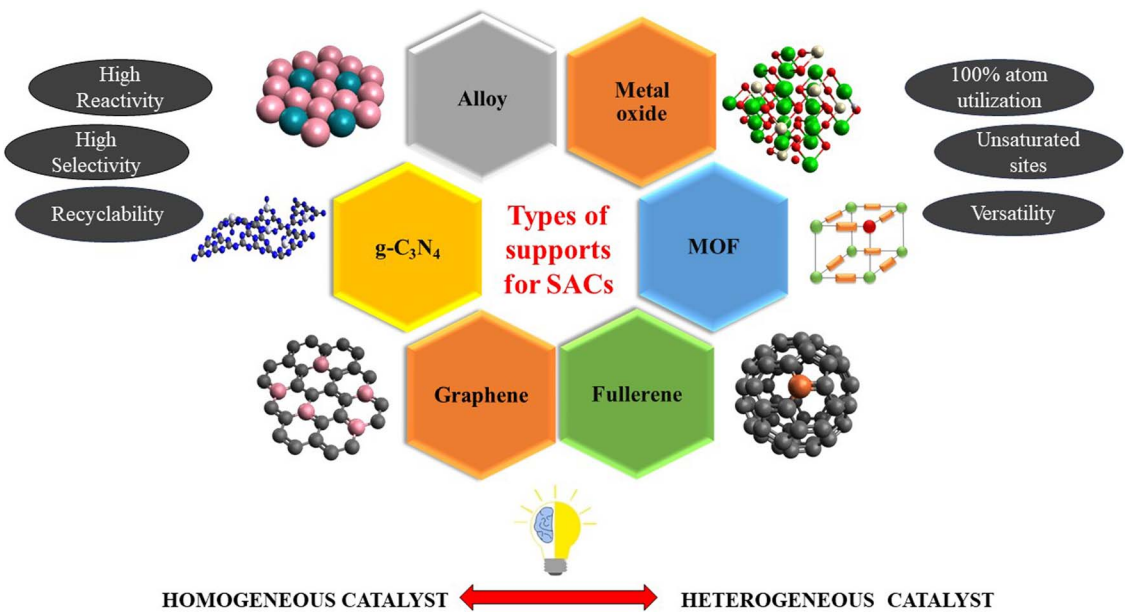

Fig. 2 An illustration of different types of support that can be used for stabilizing SACs.

carbon-based materials,[24,25] MOF,[26,27] and alloys[28,29] are needed as they promote the high dispersion of single atoms on the surface rather than in the bulk. The isolated active sites stabilized on the exposed surface of the support are responsible for the high catalytic efficiency of the SACs.[30] Fig. 2 illustrates the various types of supports extensively used for stabilizing SACs.

The atomic dispersion of the noble metals onto the surface of a suitable support promises maximum atom utilization with minimum usage for various heterogeneous reactions. The development of highly efficient SACs requires precise control over the metal content. Moreover, the coordination configuration and morphology of the supports seem to be responsible for guiding an unprecedented interaction of isolated metal atoms with the support and maintenance of high dispersion of SACs. DFT calculations are ideal for identifying the binding sites for single atoms. Fig. 3b simplifies the formation energies of atomic catalysts (EF) using the Born–Haber cycle, which helps to identify the binding sites for Cu SACs on the TiO_2 anatase phase (101). The thermodynamic driving force needs to be controlled to ensure binding in Ti vacancy sites instead of O vacancies, which was done by adopting a modified wrap–bake–peel method, as shown in Fig. 3d.[31]

2.1.1 Metal oxide supported SACs. Metal oxides, such as TiO_2, CeO_2, and ZnO, are one of the most widely used supports for ADMCs owing to the large number of hydroxyl moieties that remain on the surface of metal oxides and can act as active sites for coordinating foreign metal atoms. The O^{2-} ions on the surface of metal oxides can also behave as potential coordination sites for the single metal atoms through covalent bonds.[30–33] The high oxygen mobility of the Ce^{3+}/Ce^{4+} redox couple and its greater stability at high temperatures result in the high thermodynamic stability of CeO_2, which makes them a versatile support for anchoring the single atoms. When pure CeO_2 is used as a support for a single atom, it can store oxygen in catalytic reactions, thereby enhancing catalytic activity during oxidation reactions.[34] It has been found that the coordination structure and electronic properties of noble metals like Rh single atoms on cubic CeO_2 can be tuned using different calcinating temperatures. The high-temperature treatment of the catalyst removes the hydroxyl groups, resulting in oxygen vacancies exposing more unsaturated coordination sites of the Rh atom. The best catalytic behaviour was obtained with Rh/CeO_2 calcined at 800 °C for hydroformylation reactions.[35–37] The various possible anchoring sites for isolated atoms on the highly exposed (111) plane of CeO_2 nanocrystals are shown exquisitely in Fig. 4, which offers lower activation barriers for the dissociative adsorption and desorption of H_2.[38] This lower energy barrier for H_2 dissociation leads to its dominance for

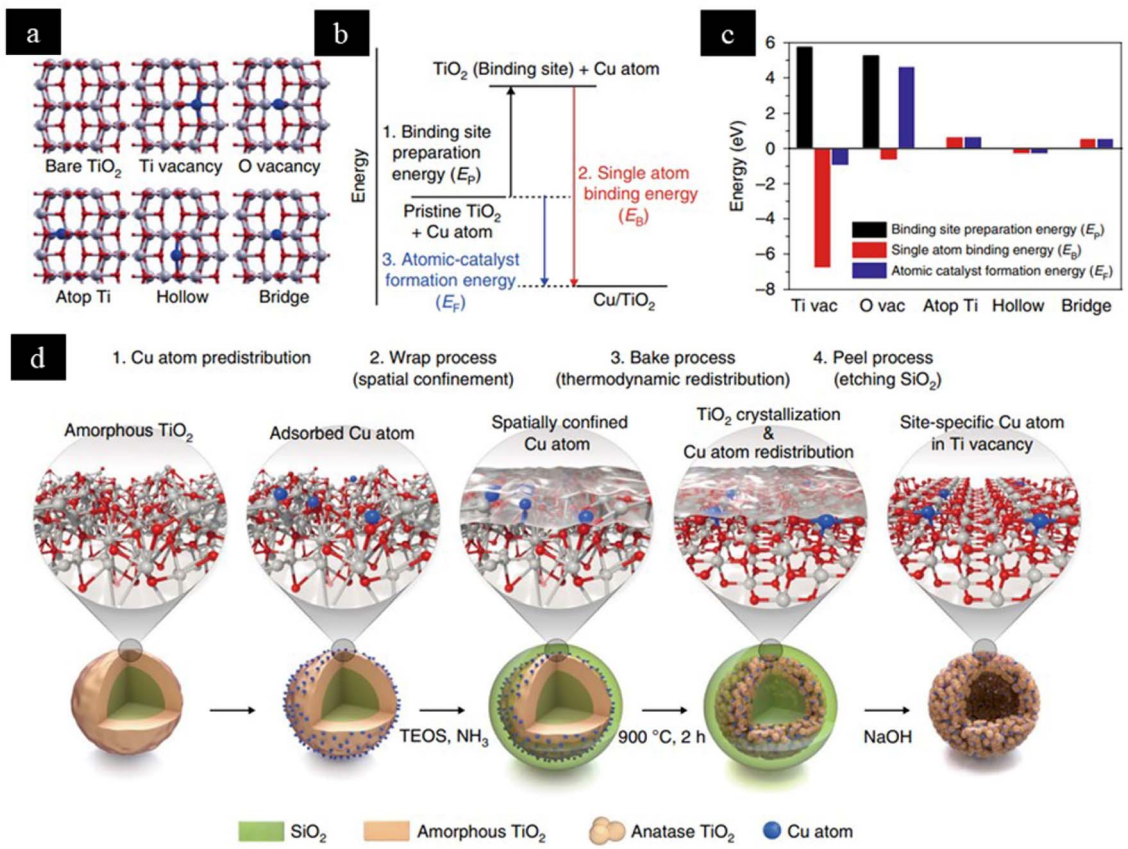

Fig. 3 A depiction of (a) binding sites for single metal atoms on a TiO_2 anatase (101) surface. (b) Born–Haber thermodynamic cycle for calculating SAC formation energies (EF): the binding site preparation energy (EP) + the single atom binding energy (EB). (c) Born–Haber energy components for possible single-atom binding sites calculated using DFT. (d) Modified wrap–bake–peel process to synthesize single-atom Cu/TiO_2 photocatalysts. TEOS, tetraethyl orthosilicate. Reproduced with permission from ref. 31. Copyright 2019, *Nat. Mater.*

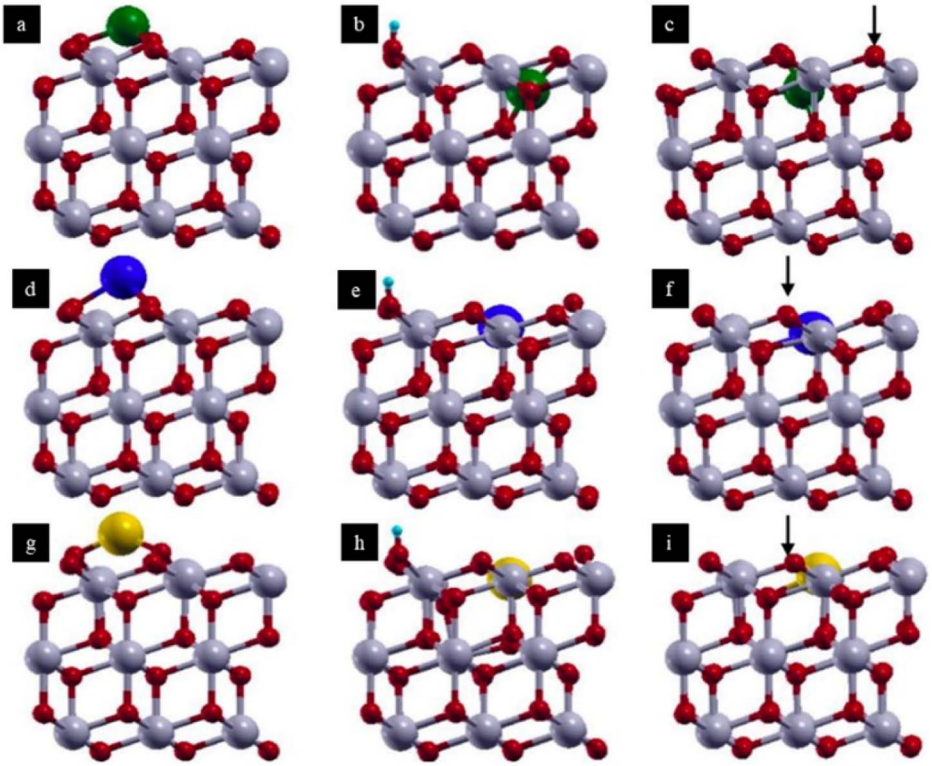

Fig. 4 A depiction of models (side views) of a supported noble metal atom M (M = Cu, Ag, Au) on CeO_2(111) investigated in this work: (a, d and g) M adsorbed on CeO_2 (M/CeO_2); (b, e and h) M substituting a Ce atom in the presence of an adsorbed H (M: H–CeO_2); (c, f and i) M substituting a Ce atom in the presence of an oxygen vacancy (M: CeO_{2-x}). Green (first row), blue (2nd row), and yellow (third row) spheres indicate the Cu, Ag, and Au atoms, respectively. Gray and red balls represent cerium and oxygen atoms, respectively. Arrows indicate the positions of the oxygen atoms that were removed. Reproduced with permission from ref. 38. Copyright 2019, *J. Phys. Chem. C*.

nitrobenzene hydrogenation over the Ni/CeO_2(111) surface.[39] The SACs supported on CeO_2(111) also show superior catalytic activities for reactions, such as methane oxidation.[40] It has been found that the rod-shaped CeO_2 with the (210) exposed planes have more oxygen vacancies compared to the (111) planes, which proves to be beneficial for high CO oxidation rates. Such morphology-controlled strategies combined with high-temperature treatments can also be used for other organic transformations owing to the higher number of active sites resulting from a higher number of oxygen vacancies on some planes of the supports than others.[41]

However, the CeO_2 support often suffers from sintering when pyrolyzed at high temperatures during the synthesis of SACs. So, UV irradiation can help efficiently stabilize the single metal atoms by avoiding the breaking of M–O bonds because of the sintering of the support material.[42,43] The "wrap bake peel method" was adopted recently to curb the sintering of CeO_2 support, as shown in Fig. 5. In this strategy, at first, they synthesized the Rh/CeO_2 catalyst, followed by wrapping it with a SiO_2 layer in order to protect it from sintering during high-temperature aging. Finally, NaOH was used to remove the surface-coated SiO_2 to yield the final Rh/CeO_2–S catalyst.[41]

A careful surface engineering of metal oxides through calcination and pyrolysis at different high temperatures and utilization of morphology-controlling agents can yield porous structures, which seem to facilitate the stabilization of single atoms on the surface.[44,45] Moreover, such high-temperature treatments often lead to the rearrangement of the nanoclusters into catalytically active single atoms, as exhibited in Fig. 6.

Maintaining control over the coordination environment of SACs is a challenging task. Secondary doping of non-precious heteroatoms, such as O, S, and P, will likely provide more coordination sites for firmly holding the single metal atoms and provide a unique coordination environment. Surfactant-assisted synthesis involving the usage of surfactants like ethylene glycol is found to control the particle size and exposed planes of metal oxides such as TiO_2. Moreover, the ethylene glycol radicals are found to be responsible for the formation of the M–O bonds and stabilizing the single metal atoms on the surface of the support material. Using HF along with ethylene glycol resulted in the exposure of perfect ratios of the exposed surfaces for hydrogen evolution reaction, thus pointing towards their morphology-controlling abilities, which can also be used for developing photocatalysts for organic reactions.[46–48] Zinc ferrite is an excellent photocatalyst for a variety of photocatalytic degradation processes. Its combination with metals like Co, Pd, Al, Pt *etc.* nanoparticles enhances their photocatalytic activity, provides more stability and prevents catalyst leaching. So, the atomic dispersion of such metals on the zinc ferrite surface can

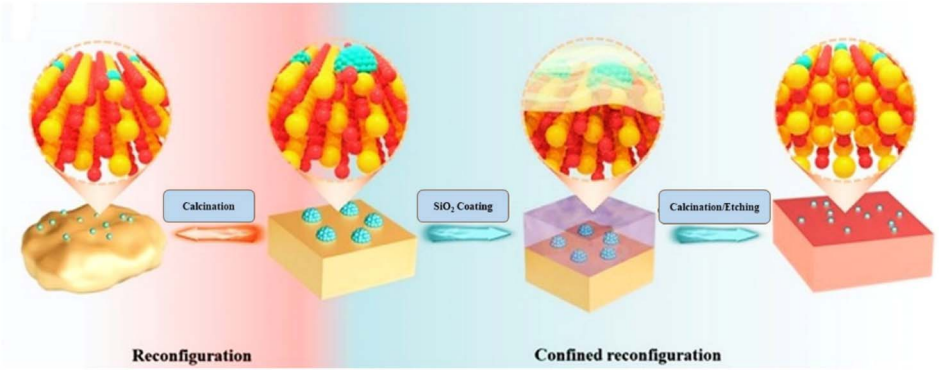

Fig. 5 Schematic representation of the "Wrap bake peel" strategy for stabilizing SACs. Reproduced with permission from ref. 41. Copyright 2023, *Angew. Chem. Int. Ed.*

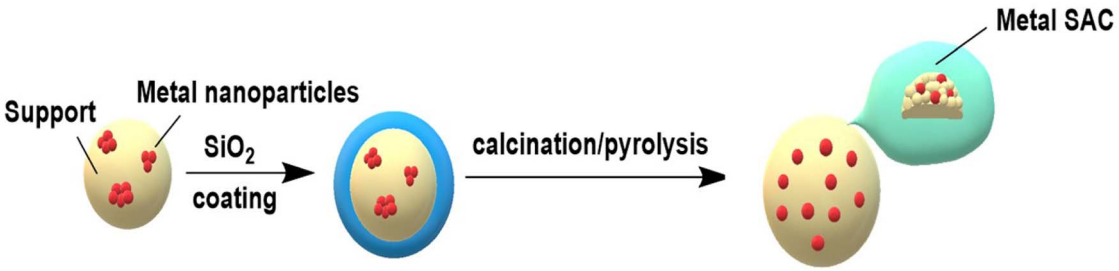

Fig. 6 A schematic representation of SAC formation *via* surface modification through calcination or pyrolysis.

be a new strategy for getting better photo-voltaic properties.[49] Low-cost and less toxic surface modifiers like SDS and L-cysteine give rise to the mesoporous structure of α-Fe_2O_3.[47] Such mesoporous structures have the potential to provide better anchoring sites and larger surface area for stabilizing the single metal atoms efficiently. However, controlling the pore size is extremely crucial as larger pores and mismatch with atomic radii might also cause clustering of the single atoms, thereby reducing catalytic activity. Dual single-atom doping of Cu and In on highly mesoporous TiO_2 exhibits superior catalytic activity for photocatalytic degradation of Cr(VI) compared to their single-atom doped counterparts, which is comparable to benchmark catalysts. This enhanced photocatalytic activity can be attributed to the synergic effects of the maximum dispersion of dual active centers and the larger surface area of the mesoporous supports.[50]

Fig. 7 depicts the benefits of morphology-controlled synthesis of SACs. A combination of hard templates with pore-forming agents provides a larger specific area and enhanced hydrophilicity, resulting in a larger number of easily accessible catalytically active sites. To determine the overall efficiency of the catalyst in any reaction, the identity of the atomically dispersed active metal is extremely important as it governs the entire reaction pathway. It has been observed that when metals like Pd, Ag, Rh, Pt, Au and Fe are used in place of Ru as single atoms on rod-shaped MnO_2, the catalytic conversion and selectivity decreases significantly for the oxidative cyanation of *n*-heptanol. This reduction in catalytic activity occurs due to the blockage of catalytically active sites of supports by these metals. Evaluation of multiple supports for the reaction also showed that the reaction occurs efficiently only on rod-shaped MnO_2 and not even on commercially available MnO_2. This result indicates the fact that it is the synergy of the type of metal used and morphology of the support material that successfully exposes a greater number of surface-active sites for the reactions.[51]

The orbital energy levels of the dopant metals can be regulated by monitoring the identity and density of the secondary dopants. Electron-donating neighbours increase the energy of the active centers and make them nucleophilic in nature, whereas electron-withdrawing neighbours make the active centers electrophilic in nature, assisting redox reactions.[48]

The general mechanism of biomass conversions like cellulose hydrolysis reveals that strong binding sites capable of breaking inter and intramolecular hydrogen bonds of cellulose must be present on the catalyst in combination with Brønsted acidic sites. So, porous supports like MOF functionalized with acidic groups like SO_3H with anchored SACs seem to be an excellent strategy to enhance the hydrolysis rate, but this aspect of morphological impact on biomass conversion rates has not yet been explored.[52] Modulation of the local microenvironment of a single atom with N and B gives rise to highly polar sites capable of activating hydrogen from the reductant while simultaneously transferring it to the acceptor C=O group. Such strategies are found to be beneficial for C–N bond formation, which is crucial for the conversion of cellulose to value-added

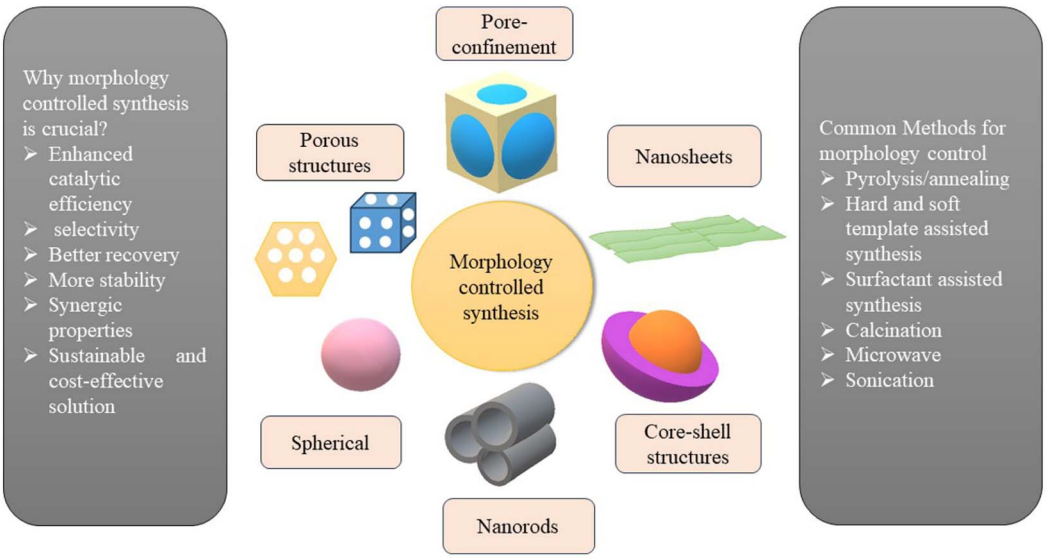

Fig. 7 An illustration of the importance and methods for morphology-controlled synthesis of supported SACs.

amines.[53] C–H activation is a very crucial step for the synthesis of a variety of chemicals and pharmaceutical products. The introduction of yttrium single atoms to the TiO_2 surface results in an increased number of oxygen vacancies and causes lattice distortion, which helps activate the surface lattice oxygen. These activated oxygen molecules directly react with benzyl radicals when irradiated under light, thus yielding benzaldehyde.[54] Such oxygen-activating properties of SACs are also beneficial for acetone oxidation reactions. Hydrothermally prepared Co single atom doped MnO_2 shows excellent catalytic activity for this reaction owing to the hydrogen-bonded complex formed between acetone and hydroxyl group resulting from easy dissociation of water.[55]

2.1.2 Metal–organic framework (MOF) supported SACs. Metal–organic frameworks (MOF) are porous crystalline materials possessing ultrahigh surface areas, well-defined, highly ordered structures and flexible tunability.[56] They are composed of secondary building units (consisting of the metal nodes and metal clusters) and organic linkers. MOF, in its original form, finds a wide range of applications in batteries, supercapacitors, photocatalysis, sensing and batteries due to its high tunability of morphology, pore size and structural modification. So, the development of MOF-based SAC is an intriguing strategy for new-age materials with tunable properties for efficient organic transformations. Metal nodes in MOF usually remain in an atomic form but not in an unsaturated state because of which they cannot act as SACs. In order to make unsaturated coordination sites available, either the solvent or water molecule must be removed or ultrathin MOF sheets need to be developed so that single metal nodes have enough unsaturated sites available for the coordination of reaction substrates.[14,57]

There are two types of MOF-based SACs:

(a) MOF supported ADMCs:

In MOF-supported ADMCs, the original MOF structure remains intact. MOF proves to be an excellent support material for developing the highly dispersed SAC as there are multiple possible ways of stabilizing single metal atoms on MOF due to their unique structure. The single atoms can be anchored onto the metal nodes or the organic linkers might provide suitable sites for anchoring. When the N-containing ligands like porphyrin and bipyridine are used as organic linkers, they promote higher loading of catalytically active single metal atoms and there have been reports of loading up to 12 wt% of Pt with the help of such interactions.[58] Moreover, the large number of well-defined pores present in MOF can also confine and stabilize the single atoms.

(b) MOF derived ADMCs:

In MOF-derived ADMCs, a new phase is formed, *i.e.*, MOF is used as a precursor for the synthesis of some other types of SACs like SAA, single atom metal oxides and heteroatom doped carbon supported single metal atoms by employing thermal treatments and chemical methods. Thermal treatments like pyrolysis often cause agglomeration of single atoms, which significantly decreases the number of catalytically active single atoms. This drawback limits the practical utility of MOF-derived ADMCs. In order to overcome this drawback, a higher number of heteroatoms like N and S needs to be introduced to hold onto the single metal atoms.[56] A MOF-derived Zn-based SAC consisting of a zeolitic imidazolate framework and Zn metal nodes was developed, which was etched to give rise to a hollow porous carbon support containing a large number of N dopants. It was then pyrolyzed at very high temperatures in order to give rise to Zn single metal atoms anchored onto the N-doped carbon support, as shown in Fig. 8. Using this strategy, they successfully loaded 11.3 wt% of Zn single atom onto the support surface, which is significantly high compared to other supports.[59] However, it seems to be a cumbersome process to synthesize MOF-derived SACs. So, developing simple, hassle-free and highly efficient synthetic routes for MOF-derived SACs is a much-needed advancement in material science.

Selective hydrogenation reactions are extremely crucial for the commercial production of various products. But, over-hydrogenation of the substrates is a major challenge during

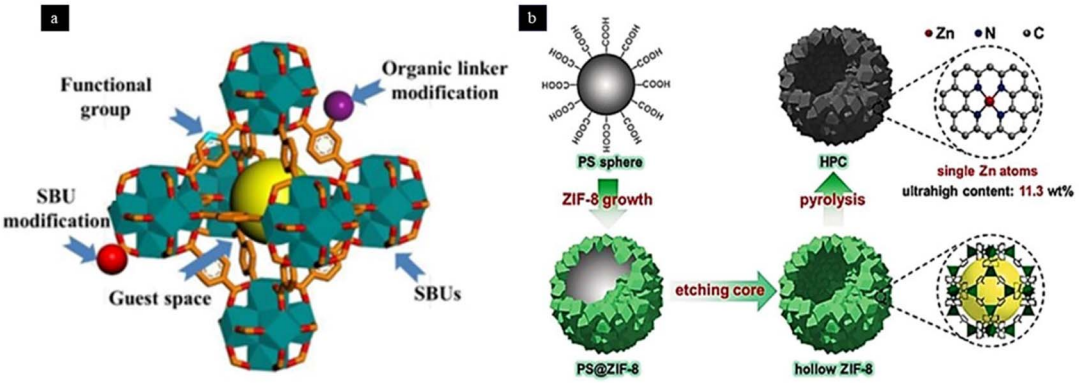

Fig. 8 A depiction of (a) different anchoring sites of an MOF. Reproduced with permission from ref. 56. Copyright 2020, *Energy Environ. Sci.* (b) Hollow porous carbon supported Zn SAC prepared from an MOF precursor. Reproduced with permission from ref. 59. Copyright 2019, *Angew. Chem. Int. Ed.*

the reaction. A comparison of the MOF-derived N-doped carbon support with other carbon supports revealed that doping with nitrogen introduces basic sites and polarizes the surface, which not only helps with H_2 dissociation but also interacts well with the polar nitro group. Simultaneously, repulsive interaction between the amine group and basic sites facilitates higher selectivity for nitrobenzene reduction to aniline.[60–62] The Co–N–C bonds are found to accelerate the hydrogenation process of nitroarenes in a mixture of protic solvents containing alcohol and water. This can be attributed to the possible H shuttling on the Co SAC surface, which facilitates the H_2 activation, followed by activated H-atom transfer to neighbouring organic ligands or molecules by alcohols.[61,62] Benzyl alcohol conversion to acids and nitriles is a highly desirable reaction for industrial production. Co–N_4 sites synthesized by the one-pot pyrolysis yield excellent results for such conversions. Similarly, N-doped carbon obtained from benzylamine modification of Fe-ZIF acts as a crystallization regulator, transforming the morphology from nanosheets to dodecagon with increased nucleation speed and crystallinity, which results in more stable Fe–N_4 anchoring sites for benzyl alcohol conversion to benzonitriles. These superior catalytic properties may arise because of the microenvironment of the single atoms flanked by four nitrogen atoms, which increase the electron density over the isolated metal centers, thereby accelerating the activation of the reactant.[63,64]

Template-assisted synthesis of MOF-derived and other supported SACs not only enhances the loading and stability of the SACs but also amplifies the number of catalytically active sites. Overhang-eave morphology, as shown in Fig. 9, is found to provide a larger surface area. When a SiO_x coating is provided to the synthesized MOF, it results in anisotropic thermal shrinkage of the MOF precursors by inducing an outward adsorption force and finally gives rise to overhang-eave structures with superior catalytic activity after the removal of the SiO_x coating.[65] Although the so-developed catalyst showed better catalytic activity for oxygen reduction reaction, such SACs with specific morphologies can also be explored for organic transformations.

Noble metals like Pd and Au are extensively used for the industrial production of benzaldehyde and benzoic acid from benzyl alcohol.[66] *In situ* formation of Pd single atoms by dissolution of <0.1 mol% of $Pd(OAc)_2$, K_2PdCl_4, $Pd(acac)_2$, and $Pd_2(dba)_3$ salts in the reaction mixture yields 50–80% of benzoic acid in just 4 hours. However, similar results are not observed for Pd salts containing stronger ligands like phosphine. Thus, the nature of the interaction between the metal center and

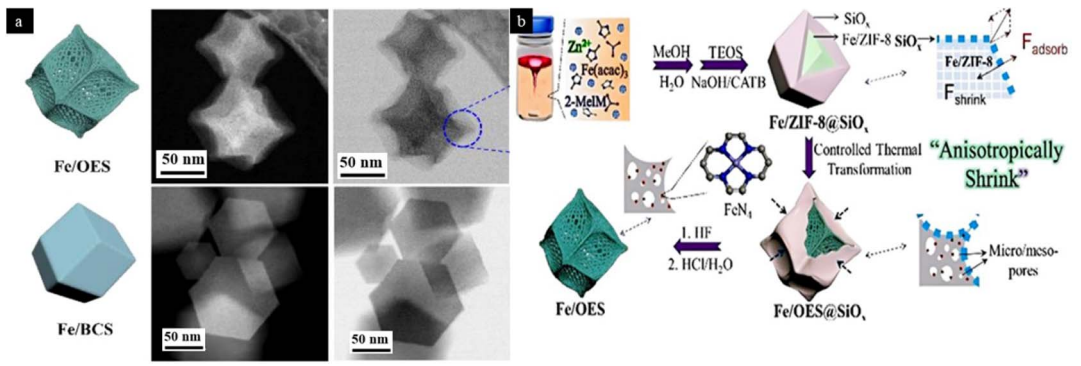

Fig. 9 An illustration of (a) HAADF- and ABF-STEM images of Fe/OES and Fe/BCS showcasing the overhang-eave-shaped structure of Fe/OES. (b) Synthetic scheme for Fe/OES. Reproduced with permission from ref. 65. Copyright 2020, *Angew. Chem.*

ligand is very crucial to deciding the activity of the SAC in soluble form. Inspired by the efficiency of the soluble form of single atoms, a Pd single atom anchored to a methyl cysteine-based MOF is used for the reaction. The incorporation of solid support successfully preserved the structure and electronic properties of SACs and prevented the leaching of the catalyst during the reaction.[67] MOFs are found to be excellent photocatalysts for a variety of reactions owing to the presence of photosensitive linkers. A comparison of photocurrent response, EIS, photoluminescence and UV-vis spectra of various samples of atomically dispersed Ni on different MOF, as shown in Fig. 10 with different coordination environments, suggests that Ni_1–S/MOF exhibits superior photocurrent response due to rapid charge transfer processes. Thus, it implies the fact that a proper combination of well-dispersed atomically active sites with modulation of coordination environment with photosensitive linkers is an excellent strategy for slowing down the electron–hole recombination process.[68]

2.1.3 Carbon-supported SACs. Carbon-based materials are versatile metal-free supports for anchoring single atoms due to their high surface area, porosity and tunable morphologies.[69] Introduction of earth-abundant heteroatoms, such as N, O, and P, into the carbon matrix results in more anchoring sites, thereby enhancing the metal loading on the surface. It is observed that as compared to the sheet-like 2D-gC_3N_4, rod-shaped morphology increases the interlayer distance, modulates the electronic properties and increases the unsaturated sites of Co single atoms on its surface. The availability of a significant number of coordination sites on the curved surface facilitates better adsorption of substrates and oxygen dissociation, which accelerates cyclohexane oxidation.[70] On the other hand, its irregular platelet-like morphology with Cu^+ ion sandwiched between its layers in linear form has shown 82% conversion with 55% selectivity for cyclohexene oxidation.[71] A sandwich structure of g-C_3N_4 exhibited a conversion of 23% with 82–92% selectivity for oxidation of cumene to cumene hydroperoxide.[72] Theoretical calculations of Gibbs free energy for the elementary steps of cumene oxidation have revealed that Fe and Co single atoms anchored onto nitrogen-doped carbon supports show superior catalytic activity as compared to Cu and Zn single atoms.[73] Thus, the coupled effect of atomic dispersion of metals with the morphology-controlled synthesis of g-C_3N_4 gives rise to unique structures, which accelerate the activation of molecular oxygen in the atmosphere and hence they show outstanding oxidative properties. Carbon-supported SACs are also beneficial for the selective oxidation of some other hydrocarbons to value-added products. However, such conversions are often difficult to achieve because of the possible activation of the C–H required for the reaction. Even though strong oxidizing agents like dichromate and permanganate are used for such reactions, they often lead to the production of large amounts of hazardous waste. Among the transition metals, Fe, Co and Mn, Co is found to exhibit the best catalytic performance for the production of acetophenone and benzaldehyde from ethylbenzene and alcohols, respectively. Atomic dispersion of Co over carbon supports like g-C_3N_4 and graphene can activate mild oxidizing agents, such as peroxymonosulfate, which gives $^{\bullet}OH$, $SO_5^{\bullet-}$ and $SO_4^{\bullet-}$ radicals upon activation. These oxidative radicals are crucial for such oxidative processes.[74,75]

2.2 Single atom alloy (SAA)

In single atom alloys (SAAs), one of the metals of the alloy remains in an atomically dispersed state. The less reactive host metal surface provides the surface defects required to fix the more reactive foreign metal into its lattice, while the ligand strength and the steric strength modulate the electronic structure of the foreign metal atoms.[76,77] For effective alloy formation, the redox potential of the constituent metal ions needs to be close to each other. Intermetallic compounds belonging to the class of alloys consist of isolated sites; however, the amount of dopant is much higher, and their ensemble is much broader. Platinum group metals exhibit excellent catalytic activity in

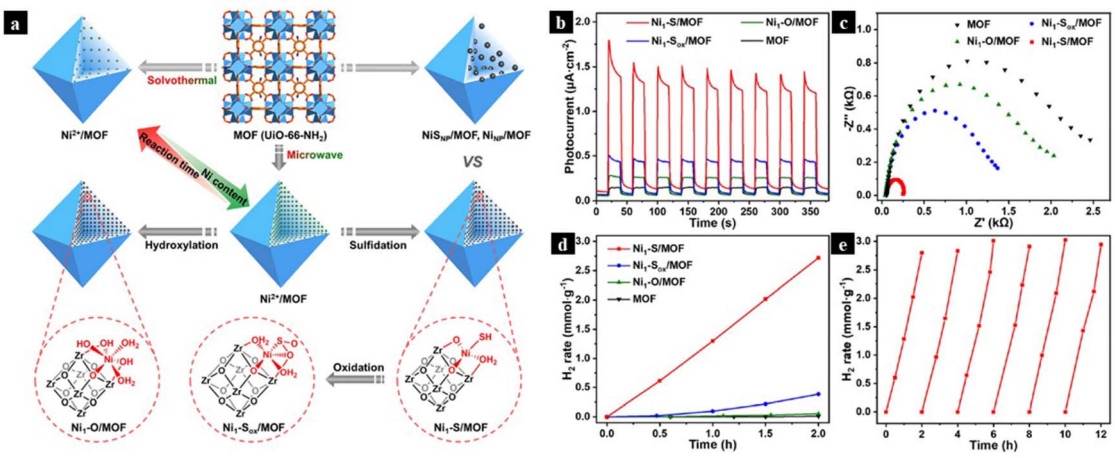

Fig. 10 (a) A schematic illustration of the synthesis of atomically dispersed Ni^{2+} on UiO-66-NH_2 using microwave-assisted synthesis, followed by modulation of coordination environment of an Ni single atom to obtain Ni_1–X in place of Ni_{NP}/MOF and NiS_{NP}/MOF. (b) Photocurrent responses, (c) EIS plots, (d) photocatalytic HER rate of Ni_1–X/MOF and MOF. (e) Recycling performance of Ni_1–S/MOF for photocatalytic H_2 production. Reproduced with permission from ref. 68. Copyright 2021, *J. Am. Chem. Soc.*

various organic transformations, but their high affinity for CO makes them extremely susceptible to poisoning. Alloying these platinum group metals through atomic dispersion with transition metals showing lower affinity for CO proves to be an excellent strategy to improve the stability of noble metal-based catalysts without compromising the activity of the catalyst.[76–78] The stability of SAAs depends on two factors- segregation energy and aggregation energy. The aggregation energy is a thermodynamic quantity that determines the relative stability of the isolated dopant atoms compared to the dopant clusters, and segregation energy determines the relative stability of the isolated atoms on the surface of the host metal rather than in the bulk. DFT calculations reveal that in most of the SAAs, the segregation energy is negative, suggesting greater stability of the single dopant atom in the bulk rather than on the surface. But, in some cases, the strong adsorbate-dopant bonds result in a higher concentration of the dopant on the surface rather than in the bulk of the surface. Pd/Cu (111) and Pt/Cu (111) are some examples of SAAs in which a higher concentration of the dopant can be observed on the surface of the host rather than in the bulk. A positive aggregation energy of the two metal atoms is necessary for the formation of SAAs. The adsorption of small molecules like CO and H_2 can control the aggregation energy as well as segregation energy, thus resulting in a greater number of single atomic sites on the surface of the host metal.[53,76] The SAAs exhibit unique dual-site catalytic behaviour, which helps in catalyzing different elementary reactions of an organic transformation.[77] It has been observed that Pd containing SAAs shows exceptional catalytic activity for selective hydrogenation reactions of various organic compounds. Unlike monometallic Pd nanoparticles where desorption of dissociated H atoms becomes a challenge, isolated Pd atoms cause the dissociation of H_2 molecules on its surface, followed by the spillover of the dissociated H atom to the host metal, thereby facilitating its faster desorption from the catalyst surface. PdCu, AgPd, RuNi, PdAu and PtCu SAAs are some of the highly effective combinations of metals for chemoselective hydrogenation of acetylene, levulinic acid, nitroarenes, styrene, olefins and many more.[77–82] SAA, like PtCu, also facilitates C–H activation, which is crucial for cyclic hydrogenation and dehydrogenation reactions without any coke formation. DFT calculation reveals that the synergy of such a combination of metal species results in a balance of binding forces for intermediates, leading to hydrogenation on Pt and dehydrogenation due to Cu centers.[83] The synthesis of most of the SAAs requires the assistance of reducing support materials like alumina, silica and N-doped C-supports. Therefore, the development of self-assembled SAAs would represent a novel approach in this field. Methods such as leaching result in stable self-assembled SAA, thereby making the process more hassle-free.[48,53,76–78,84]

3. Impact of defect engineering and piezocatalysis on the efficiency of SACs

Defect engineering of supports helps with the customization of vacancy defects, edge defects and dopant-derived defects.[85,86] Pd single atoms anchored on oxygen vacancies of CeO_2 nanorods synthesized from defect engineering of supports exhibit 99% conversion and exceptional turnover frequency for the selective hydrogenation of styrene and cinnamaldehyde, as well as triethoxysilane oxidation. Unlike Pd nanoparticles, confining Pd single atoms on oxygen vacancies exposed a greater number of unsaturated sites for easy dissociation of H_2, which helped accelerate the hydrogenation process without causing any leaching of the catalyst during the reaction.[87] Selective oxidation of methane to C_1-oxygenates is a crucial reaction for the synthesis of a variety of value-added products. But, this reaction often suffers from loss of activity and selectivity due to the formation of large amounts of by-products. Low temperature (<200 °C) methane conversions are found to be ideal for more efficient utilization of methane. The introduction of carbon vacancies and P dopants adjacent to Fe–N_4 sites on graphene sheets is found to significantly enhance methane conversion at room temperature. This significant increment in its catalytic properties comes from the introduction of defects, which not only reduce G_f but also oxidise Fe–N_4 sites to O–FeN_4–O sites, which act as potential active sites for methane oxidation.[88]

Removal of linkers and clusters *via* the modulator approach, a mixed linker approach or post-synthetic treatment of MOFs helps in increasing the distance between the active metal centers, and at the same time, leaves a greater number of unsaturated sites available for catalytic reactivity, thus resulting in SACs. MOF-derived Co SACs were prepared *via* MOF defect engineering, followed by carbonization and acid etching in which they introduced H_2O for causing competitive coordination with carboxylic acid, thus resulting in crystal nucleation and inhibition ingrowth, ultimately giving rise to crystal defects, as shown in Fig. 11.[89] But there is a huge room to develop MOF-based SACs based on this strategy. It has been observed that the combination of a thermostable and a thermolabile linker followed by the selective removal of thermolabile linkers results in hierarchical porous structures and the degree of porosity can be controlled by using different lengths and concentrations of modulators. Also, it has been found that using potassium hydroxide and propionic acids results in missing linkers, clusters, and extra framework cations and hence these defects can be used to generate MOF-based SACs. Plasma etching is a green technique to generate vacancy defects in MOF without destroying the original framework, which can also be used to generate MOF-based SACs. The realm of defect engineering potentially results in a highly porous structure and a high specific area of defective MOF, which will allow the substrates to reach the catalytically active single metal atom efficiently.[90]

Using MOF and some metal oxides as piezoelectric catalysts is emerging as a promising approach for various energy conversions. Most piezoelectric catalysis processes seem to require the assistance of a sacrificial agent, which is not that cost-effective. However, the pore size of MOF can be altered by using flexible organic linkers of different lengths. Moreover, organic molecules that can change their conformations upon external stimuli light irradiation can be incorporated within the pores of MOF bonded to organic linkers. This strategy helps generate photoswitches, which will be beneficial for catalyzing

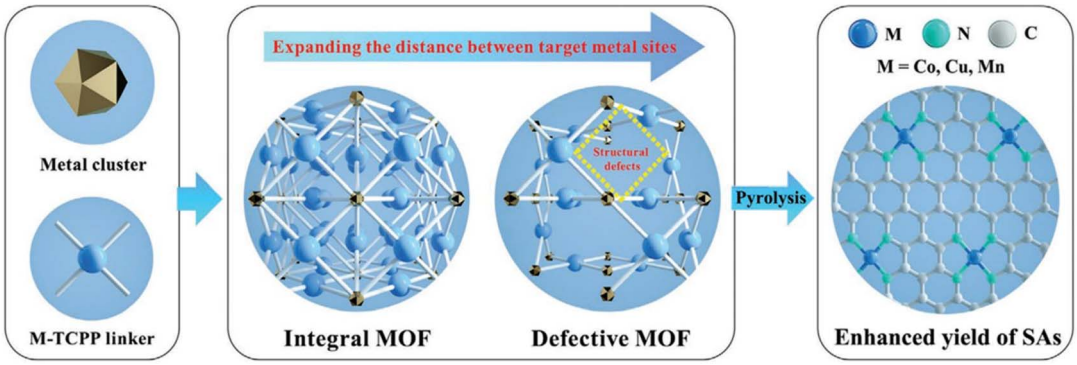

Fig. 11 A schematic of the synthesis procedure for metal SACs through the defect engineering strategy in MOFs. Reproduced with permission from ref. 89. Copyright 2021, *Adv. Funct. Mater.*

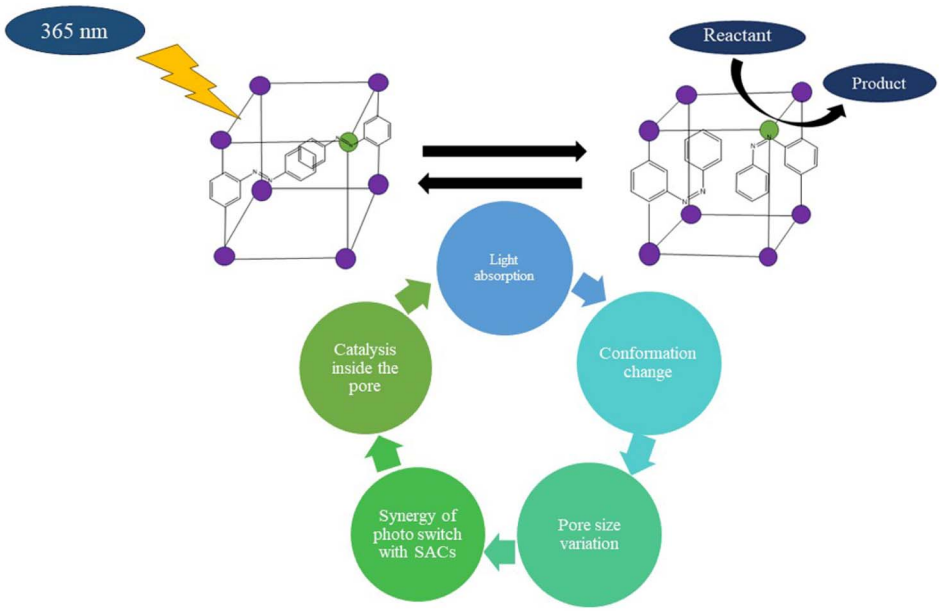

Fig. 12 An illustration of a plausible mechanism for SAC-based photoswitches.

various photocatalytic reactions inside the pores of the MOF.[91,92] The concept of photoswitches can be combined with SACs, as shown in Fig. 12, which will facilitate the electron transfer process and result in a highly efficient photocatalyst.

Fig. 13 depicts the use of piezo photocatalysis using an integral system of single Ag atoms with a piezoelectric material SnO_2 giving rise to a z-scheme heterojunction. Such systems are found to be highly beneficial for the activation of small molecules like O_2, H_2O *etc.* So, there is an urgent call for the extensive use of such catalyst applications in the field of organic transformations as well.[93]

Morphological studies on SAC-promoted piezocatalysis can open new doors of research in sustainable chemistry. It has been observed that ellipse and pyramid-shaped ZnO shows excellent piezoelectric behavior, probably owing to the growth of crystals along (002) containing a greater number of particles along the *c*-axis, which is important for ZnO to show the piezoelectric behaviour.[32,94] The incorporation of active metal SACs onto such morphology control piezoelectric material can be a leap forward for energy-efficient industrially important organic transformations. Table 1 summarizes the synthesis of various morphologically controlled SACs for organic reactions. It is clear from Table 1 that the same materials with different morphologies are highly selective for different reactions. Such comparative studies help better understand the impact of morphology on reaction mechanisms. It also depicts the growing trend and versatility of carbon supports for diverse organic transformations.

4. Application of atomically dispersed metal catalysts for industrially important organic transformations

The high efficiency and cost-effectiveness of the ADMCs have drawn the attention of the scientific community in recent years.

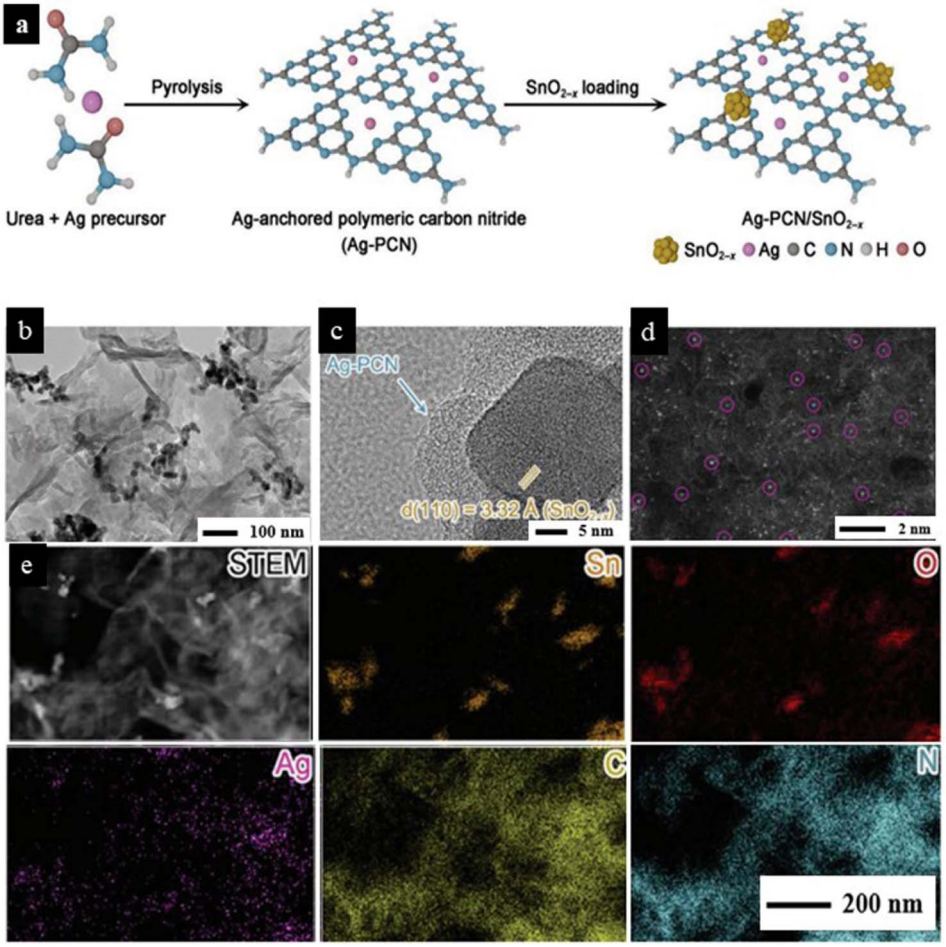

Fig. 13 (a) Schematic representation of the synthetic process of Ag atoms-anchored polymeric carbon nitride (Ag–PCN)/SnO_{2-x}. (b) TEM and (c) high-resolution TEM (HRTEM) images of Ag–PCN/SnO_{2-x}. (d) The spherical aberration-corrected high-angle annular dark-field scanning TEM (HAADF–STEM) image of Ag–PCN/SnO_{2-x}. The purple circles highlight some of the single Ag atoms (bright dots). (e) STEM image of Ag–PCN/SnO_{2-x} and the corresponding energy-dispersive X-ray spectroscopy (EDS) elemental mapping profiles showing Sn (orange), O (red), Ag (purple), C (yellow), and N (blue) distributions. Reproduced with permission from ref. 93. Copyright 2023, *Adv. Sci.*

Table 1 A comparative study of the morphology-controlled synthesis of SACs for various organic reactions

Metal	Support	Morphology	Organic transformation	Reference
Rh	CeO_2	Nanowires	Oxidation of methane	95
		Cube	Hydroformylation	35
	Exfoliated g-C_3N_4	Sheet-like	Hydroformylation	96
	N and P-doped carbon	Polyhedra	Carbene N–H bond insertion	97
	N-doped carbon	Rhombohedral dodecahedron, nanorod	Formic acid oxidation	98 and 99
Pd	N-doped carbon	Hollow nanosheets	Suzuki cross-coupling reaction	100
		Nanosphere	Semihydrogenation of acetylene	101 and 102
Ni	Carbon nitride	Sheet-like	Photoredox C–N coupling	103
		Mesoporous	Photocatalytic C–O coupling	104
Co	N-doped carbon	Dodecahedral	Dehydrogenation of formic acid	105
		Concave	Coupling of alcohols	106
	g-C_3N_4	Rod-shaped	Cyclohexane oxidation	70
	Carbon nitride	Laminar shape	Oxidation of alkylaromatics	107
Cu	g-C_3N_4	Irregular platelet-shaped	Cyclohexene oxidation	71
	Boron nitride	Nanofibers	Nitroaromatics reduction	108
RuNi	Al_2O_3	Hierarchical	Hydrogenation of nitroarenes	77
Pt	TiO_2	Nanosheets	Hydrogenation of nitrostyrene	109

Industrially important organic transformations like the C–C cross coupling reaction, hydrogenation reactions, oxidation reactions, biomass conversion, and azide–alkyne cycloaddition reactions are crucial for the production of various value-added products. Biomass is mainly composed of carbohydrates, lipids and proteins, which consist of carbon, hydrogen and oxygen as its prime elements. The focal point of their conversion to value-added products is the selective breaking and formation of numerous C–C bonds between two different organic molecules. So, catalysts that display high activity and selectivity towards the C–C cross coupling reaction can also potentially show better results for biomass conversions. Furthermore, the azide–alkyne cycloaddition reaction, which is central to click chemistry, is pivotal for sustainability, and the catalysts used for this reaction often aim for high efficiency. So, Cu ADMCs used for azide–alkyne cycloaddition reactions with superior and unique properties can help broaden the scope of these reactions for better utility of biomass-conversion.[7,8,110–112] But, it has been seen that they often require harsh reaction conditions like long reaction times, high pressure, or large amounts of catalyst to give high yields.[113] So, the development of a cheaper alternative to the traditional catalyst that can provide high efficiency without compromising environmental well-being has become extremely crucial.

4.1 Biomass conversion

In recent years, people have become more aware of the depletion of natural fossil fuel reserves. Shifting chemical processes towards a greener approach using renewable resources and substrates has become essential to protect Mother Nature. Biomass conversion is one such process that has the potential to yield green energy and industrially important products without harming the environment. Noble metal-based nanoparticles like Pt, Ru, Au and Pd have proven to be excellent catalysts for such reactions; however, the low availability, high cost of noble metals, harsh reaction conditions and agglomeration or leaching of the synthesized catalyst remain a challenge. Hydrogenation of cellulose-derived levulinic acid (LA) to γ-valerolactone (GVL) is a highly important organic transformation because the so-obtained product γ-valerolactone (GVL) is used in the manufacture of gasoline blenders, biorefining solvent, energy-dense fuel additives and can also be transformed into intermediates of biopolymers.[114–116] This reaction involves simultaneous C=O bond activation and H_2 dissociation, which requires electron-rich catalytic centres. Many researchers have worked on the development of electron-rich Ru nanoparticles anchored onto supports like graphene oxide, N-doped C, hierarchical porous carbon and many more because of the captivating properties of Ru over other Pt group metals but the activity and efficiency of electron-rich Ru nanoparticle-based catalysts are not so appreciable because only the surface Ru species can activate C=O and cannot cause simultaneous H_2 evolution along with C=O activation, which is a very important step of such biomass conversions.[116] To overcome this drawback of Ru-based catalysts and maximize the benefits of utilizing Ru species, a MOF-derived RuCo SAA containing electron-rich Ru atoms as the active centers was synthesized for the reaction. It was stabilized onto an N-doped carbon support *via* pyrolysis. SAA formation with less electronegative Co involves electron transfer to Ru, giving rise to electron-rich Ru species that are important for efficient catalysis. The lower melting point of Co leads to their agglomeration into larger nanoparticles during pyrolysis, causing the dispersion of highly unsaturated Ru into its lattice matrix in atomic form. So, a less electronegative host metal with a low melting point is ideal for the formation of SAA catalysts for such reactions. Also, Co–N–C sites accelerate the process of H_2 activation, as previously discussed in this work, which plays a key role in the hydrogenation of LA to GVL. Their synthesized catalyst with 1.1 wt% of Ru loading exhibited a whopping turnover frequency of 3500 h^{-1}, higher than other Ru-based catalysts. Fig. 14 illustrates the mechanism involved in such conversions.[117]

Lignin degradation involving selective cleavage of C–C bonds is an extremely important reaction for the synthesis of high-value aromatic compounds and the production of fuels. The high dissociation energy of the C–C bond (226–494 kJ mol^{-1}) as compared to the C–O bond (209–348 kJ mol^{-1})[118] makes the selective dissociation of C–C linkage difficult. Electrocatalytic oxidative lignin degradation is a promising approach over other methods like pyrolysis, reduction and hydrolysis because it results in higher yields under mild reaction conditions while supporting sustainability. Moreover, electrocatalytic oxidation also results in the generation of value-added H_2 at the cathode as a by-product. It is observed that the traditional metal and metal oxide-based electrocatalyst suffers from low product yields as well as poor selectivity. So, considering the challenges faced during the degradation of lignin, the potential of SACs for electrocatalytic lignin degradation was explored. A highly efficient single atom Pt catalyst anchored onto the surface of N-doped carbon nanotubes was designed successfully for selective cleavage of the Cα–Cβ bond. Based on DFT calculations, as shown in Fig. 15f and g, they concluded that, unlike the previously reported catalysts, the synthesized Pt_1/N-CNTs electrocatalyst proceeded through the formation of Cβ radical intermediate in place of Cα ketone or Cα radical intermediates, which then induced highly selective Cα–Cβ bond cleavage by coupling with $^tBuO^{\bullet}$.[119]

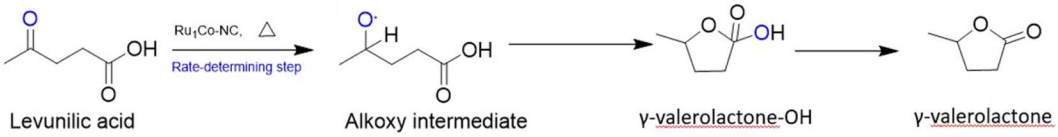

Fig. 14 Schematic of levulinic acid conversion into γ-valerolactone catalyzed by Ru_1Co-NC SAC.

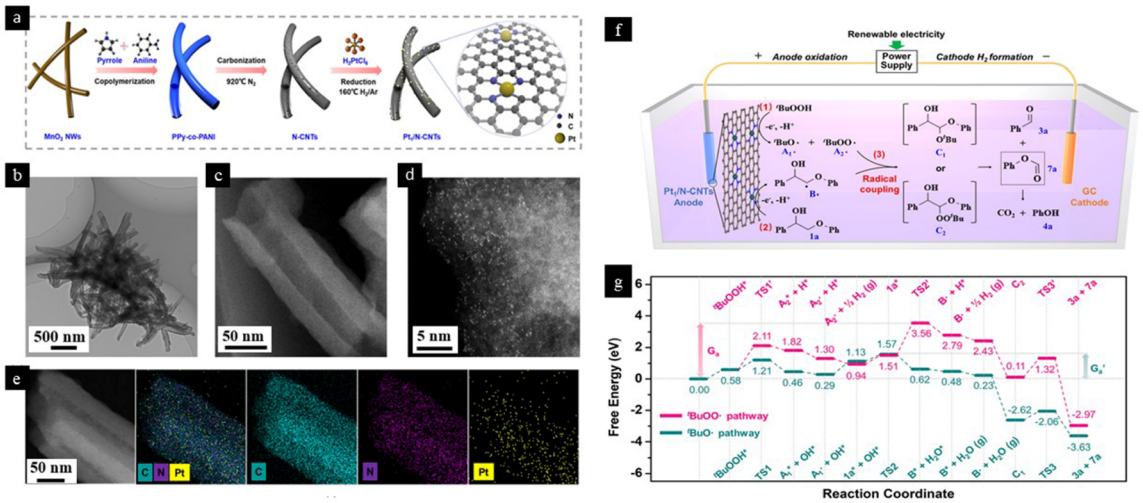

Fig. 15 A depiction of the proposed strategy and characterization of the Pt_1/N-CNTs catalyst. (a) Schematic of the preparation of Pt_1/N-CNTs. (b) TEM image of Pt_1/N-CNTs. (c) HAADF-STEM image of Pt_1/N-CNTs. (d) Representative AC HAADF-STEM image of Pt_1/N-CNTs. (e) EDX elemental mapping analysis of Pt_1/N-CNTs, structural identification of a Pt single atom in the Pt_1/N-CNTs catalyst, (f) proposed mechanism of the Pt_1/N-CNTs-catalyzed conversion based on experiments and DFT calculations (g) DFT-calculated potential energy surface for the reaction on the Pt_1/N-CNTs surface. Reproduced with permission from ref. 119. Copyright 2021, *J. Am. Chem. Soc.*

The electro-oxidation of 5-hydroxymethyl furfural (HMF) not only yields a variety of value-added products but also can serve as an alternative anodic reaction that has the potential to improve the sluggish kinetics of reactions such as oxygen evolution reaction (OER). Successful loading of about 0.5 wt% of Ru single atom was accomplished on ultrathin nanosheets of CoO_x. The high dispersion of Ru was ensured with the help of lyophilization. They found that the selectivity and yield obtained with their synthesized catalyst for electrooxidation of HMF were 13.8% and 13.3%, respectively, which was more than CoO_x.[120] This enhanced catalytic activity can be attributed to the synergy of SAC and the support. The highly unsaturated sites of the SAC might facilitate greater adsorption of the substrate onto the surface of the catalyst, thereby providing a lower energy barrier for C–H bond activation, which is the rate-determining step for the electrooxidation of HMF. Moreover, it is also observed that precise modulation of the coordination environment of the single atoms through its combination with various other desirable metals leads to a synergic effect, which might help in overcoming the drawbacks of their individual counterparts. The incorporation of single atoms into the host material sometimes also alters the rate-determining step of the conventional reactions, as evident from the electrooxidation of hydrazine. Thus, a good understanding of the impact of the coordination environment of the single atom on the reaction mechanism might open new doors of exploration for their application in biomass conversion as well.[121,122] The mechanistic study of hydrodeoxygenation of lignin derivatives by H. Guo and co-workers suggests the importance of atomic isolation for controlling the adsorption modes of substrates for enhanced conversion and selectivity. Anchoring isolated Ni on Mo_2C changes the geometry of the adsorbed intermediate from vertical to horizontal, resulting in an alternative reaction pathway with a lower energy barrier.[123] A similar observation was also obtained by Y. Lu and co-workers when they used Ir SAC supported on Co_3O_4 as a catalyst for the electrooxidation of HMF. The LSV curve showed a record low onset potential (1.15 V_{RHE}), whereas Co_3O_4 and IrO_2 exhibited a comparatively higher value of onset potential (1.35 and 1.48 V_{RHE}, respectively). These lower onset potentials at higher current densities can be attributed to the preferential adsorption of C=C of the furan ring on the Ir single atom and C=O on the adjacent Co atom of the support. The temperature-programmed desorption (TPD) measurements reveal that the desorption temperature of ethylene molecules is higher on Ir_1/Co_3O_4 than on Co_3O_4. But, in the presence of a CO atmosphere, the reverse takes place. The concentration of the intermediate on their synthesized catalyst is also found to be less as compared to the support, which ultimately results in the fast kinetics of the oxidative process.[124]

Nb_2O_5 containing Nb(v) has also been proven to be a great support material for anchoring Ru atoms onto its surface for selective conversion of lignin to arenes. The porous material so formed helps with the deprotonation of C–OH groups and the phenoxide ion is bonded to the vacant sites of the synthesized catalyst, which ultimately results in the selective activation of the C–O bonds.[125] However, there are certain reports where porous supports like g-C_3N_4 encapsulated the active metal species in between its layers, ultimately reducing the catalytic activity. Thus, selecting a suitable support material that can expose most of the catalytically active sites for the proper binding of the substrates is extremely important for the reaction to proceed effortlessly.[126] In biomass conversions, very harsh hydrothermal reaction conditions are often used, so hydrothermal stability of the synthesized SACs plays a crucial role in efficient catalysis. Moreover, biomass consists of a variety of functional groups and heteroatoms, which have a very high tendency to form complexes with isolated doped metals, which might result in rapid leaching of the developed SAC, thus limiting their recyclability.[127] Core–

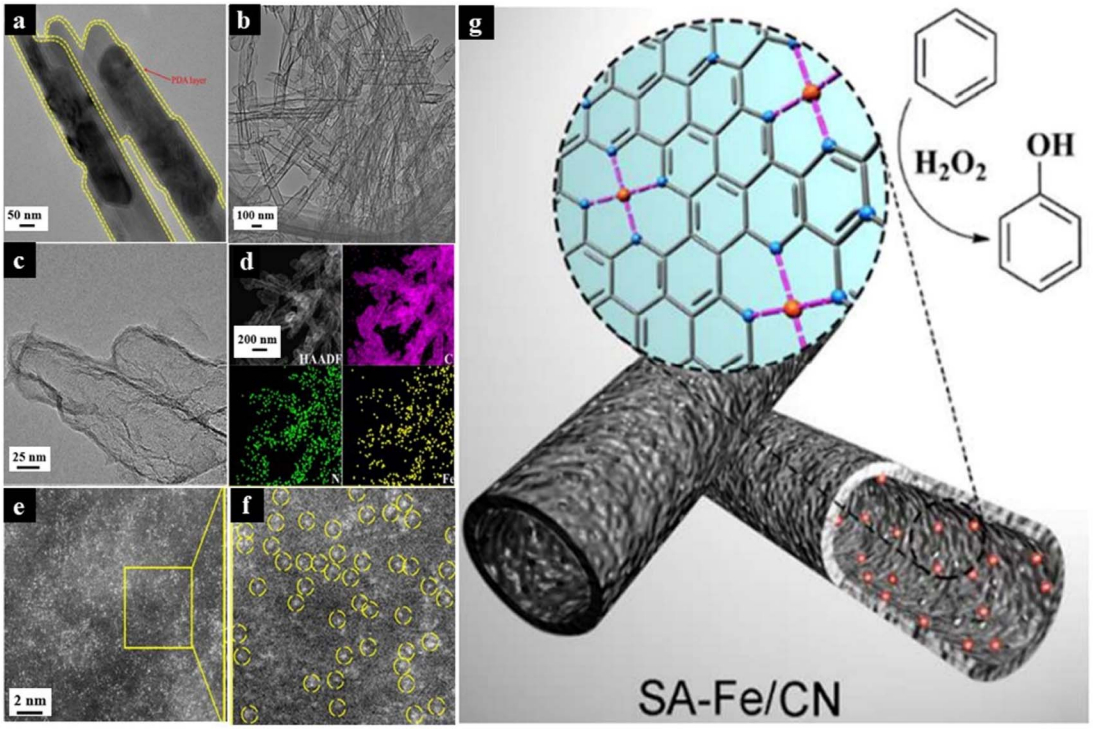

Fig. 16 TEM images of (a) α-FeOOH@PDA; (b and c) SA-Fe/CN. (d) HAADF-STEM image and corresponding EDX mapping of SA-Fe/CN, C (pink), N (green) and Fe (yellow). (e and f) AC HAADF-STEM image and enlarged view of SA-Fe/CN. (g) An illustration of core–shell structured SA-M/CN materials for direct hydroxylation of benzene to phenol. Reproduced with permission from ref. 130. Copyright 2017, *J. Am. Chem. Soc.*

shell structures with higher stability and extensive charge transfer between the layers can hold onto the SACs firmly and also promote photocatalytic biomass conversion when the shell is composed of light-harvesting systems.[128,129] Fig. 16 illustrates the TEM images of a core–shell structured Fe-based SAC prepared by pyrolysis and further leaching of PDA-coated α-FeOOH. This work emphasizes the importance of core–shell structured SACs for direct hydroxylation of benzene to phenol. Such strategies can also be extended for other industrially important organic transformations.[130]

Reactions involving the conversions of furfural to more value-added products are found to be catalyzed highly efficiently by noble metal nanoparticles like Au and Cu supported on CeO_2 nanorods. The high catalytic activity of these catalysts is attributed to the (100) and (110) exposed planes of Au/CeO_2 and Cu/CeO_2. This is because these planes are found to have the highest content of oxygen vacancies, which facilitates the easy absorption of oxygen species. The metal nanoparticles are stabilized by surface oxygen vacancies with simultaneous oxidation by adsorbed oxygen species, resulting in cationic metal species. Although such metal oxide-supported nanoparticles often exhibit satisfactory results, the SACs exhibit a better dispersion of active metal centers. These cationic metal centers are extremely crucial for C–H bond activation, which is one of the major steps for furfural conversions, as shown in Fig. 17j.[131] Thus, understanding the mechanism of the reactions will provide us with insight into the morphological requirements of the catalyst for utmost efficiency. Such a plane-specific strategy can also be used for stabilizing the single metal atoms onto the surface of metal oxides by controlling the morphology of the supports through surfactant-assisted techniques so that more plane-specific strategies can be used for catalyzing conversions.[132–134]

The combination of SACs with the conventional heterogeneous catalyst has the potential to exhibit excellent photocatalytic biomass conversion, as depicted in Fig. 18, but it still needs much exploration. One of the most difficult tasks for achieving highly efficient photocatalytic biomass conversion is to obtain highly valuable products with high selectivity without causing complete mineralization of the substrate into CO_2 and H_2O. The presence of oxygen promotes the mineralization of various reactive oxygen species into CO_2 and H_2O. The incorporation of single atoms into suitable semiconducting support not only results in unique bandgap properties but also helps control the composition and coordination environment so that a highly selective photocatalyst can be developed for each reaction pathway. It has been observed that the combination of suitable metal atoms in the form of SAA results in better adsorption at substrates due to the high surface energy and unsaturated sites, along with reduced coke formation, thereby lowering the energy barrier for C–H bond activation. Such supporting information reflects the potential of SACs to be used for highly selective photocatalytic biomass conversions, as C–H bond activation is one of its crucial steps.[135–140]

The anchoring of Ni single atoms on the surface of TiO_2 is proven to exhibit superior catalytic activity for C–C bond cleavage, which seems to be beneficial for biomass conversions.

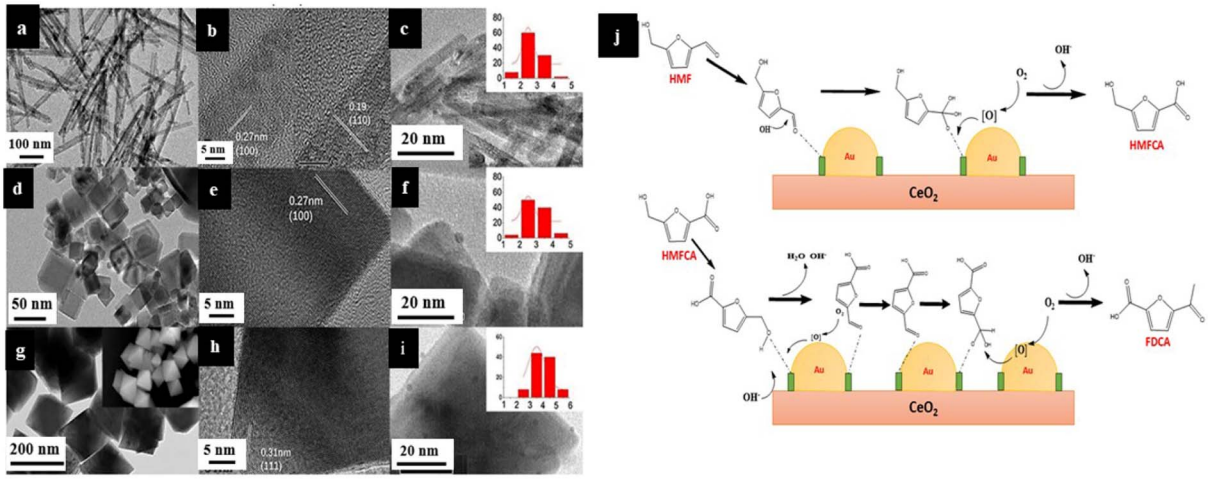

Fig. 17 Transmission electron microscopy (TEM), high-resolution transmission electron microscopy (HRTEM) and scanning electron microscopy (SEM) images: (a and b) CeO_2-rod, (d and e) CeO_2-cube, (g and h) CeO_2-oct, (c) Au/CeO_2-rod, (f) Au/CeO_2-cube and (I) Au/CeO_2-oct. The insets of (c), (f) and (i) indicated the statistical distribution of Au particles. The inset in (b) shows a zoom-in image in the (110) lattice fringe. The inset in (g) shows the SEM images of CeO_2-oct. (h) Possible reaction mechanism for oxidation of HMF to FDCA. Reproduced with permission from ref. 131. Copyright 2019, *Catal. Sci. Technol.*

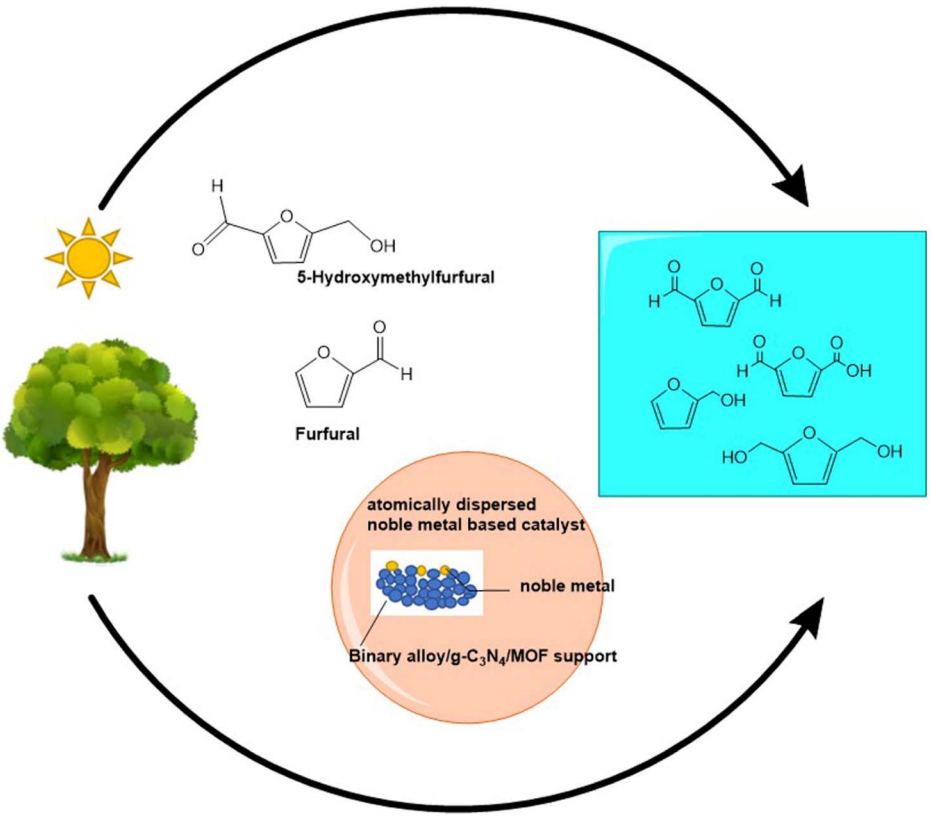

Fig. 18 An illustration of photocatalytic biomass conversion.

This enhanced photocatalytic activity arises because of the introduction of new vacant states near the conduction band of TiO_2, which not only acts as the acceptor of photogenerated electrons but also acts as an active centre for the activation of molecules. The isolated active centers, due to their highly dispersed nature, lower steric hindrance and precisely controlled local environment, help with tailoring highly selective photocatalysts for the desired organic transformations.[137–140]

The selective hydrogenation of unsaturated aldehydes and ketones in the presence of –C=C– is highly desirable and

challenging for biomass conversions. However, the isolated environment and unique binding modes of the substrate on the active metal center of SACs facilitate such conversions. A pocket-like structure of Rh_1/MoS_2 SAC is found to exhibit 50% higher selectivity towards hydrogenation of crotonaldehyde to crotyl alcohol without reducing the –C=C– as compared to their nanoparticle counterpart. The dominant absorption peak at 2090 cm^{-1} in *in situ* CO-drifts indicates the atop adsorption configuration of CO on Rh atoms anchored to the edge sites of 2D MoS_2 nanosheets. This top-on adsorption of the crotonaldehyde molecule is exothermic by 0.70 eV and stabilized by 0.18 eV, which increases the probability of such adsorption modes by 99%. DFT calculations also reveal that the η^1 mode of adsorption is much more favourable than the η^2 mode of adsorption, which results in higher chemoselectivity of SACs compared to their nano-counterparts.[141]

4.2 Hydrogenation reactions

Hydrogenation reactions are central to the petrochemical, fine chemicals and coal industries. About one-fourth of industrially important organic transformations include at least one hydrogenation step. Selective hydrogenation of aldehydes and ketones in the presence of –C=C– is crucial for various flavouring, perfume and pharmaceutical industries.[142,143] α,β-Unsaturated aldehydes/ketones are often adsorbed at the active centers through the di-σ or π mode. They can also get co-adsorbed through 1,4-di-σ modes. All these adsorption modes result in the preferential reduction of –C=C– due to thermodynamic and kinetic reasons. But, as mentioned in Sections 2.2 and 4.1, the synergy of H_2 molecule activation followed by its spillover and unique η^1 mode of adsorption on SACs helps achieve such energetically demanding selective hydrogenation.[77–80,144–146] Fig. 19 depicts the different binding modes of α,β-Unsaturated aldehydes/ketones on nanoparticles and SACs, showcasing better chemoselectivity of SACs over other nanocatalysts for the hydrogenation process.

Semi-hydrogenation of acetylene to produce plastics is extremely crucial for polymer-based industries. The three most common side reactions hindering the hydrogenation process of alkynes to alkenes are the hydrogenation of alkenes to alkanes, oligomerization of alkynes and intermediates to higher hydrocarbons and coke formation.[147,148] It has been observed that SACs promote the chemoselective hydrogenation of acetylene to ethene without causing further hydrogenation. This enhanced chemoselectivity can be attributed to the two most unique properties of SACs-ensemble effect and active site isolation. Based on the number of metal atoms present in an ensemble, there are three modes of adsorption for alkynes whose adsorption strength decreases in the order of ethylidyne on 3-fold Pd-sites > di-σ on bridged Pd dimers > π-bonded on isolated Pd single atoms, as shown in Fig. 20. Among the three modes of adsorption, it is found that the desorption energy for ethylene molecules is lower as compared to the hydrogenation process, by which ethylene molecules desorb from the surface of SACs as soon as it is formed, thus preventing unwanted side reactions.[124,141] It is found that hierarchically hollow structures of supports provide an abundant number of channels for better mass transport with a greater number of exposed sites, which proves to promote transfer hydrogenation of nitroarenes. This is also supported by the fact that hollow pocket-like structures of supports, as mentioned in Section 4, help enhance the chemoselectivity of hydrogenation processes by providing steric hindrance to side reactions. The strategy of enclosing SACs within such porous structures is adopted from enzyme catalysis, where their pocket-like structures successfully protect organic

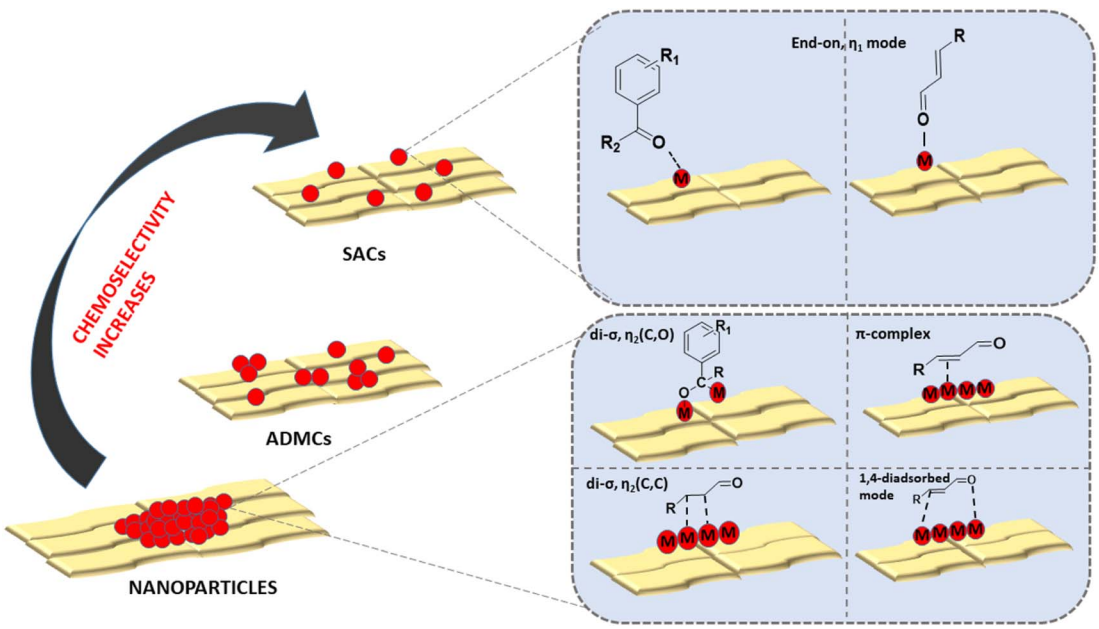

Fig. 19 An illustration of different binding modes of α,β-unsaturated aldehydes/ketones on nanoparticles and SACs for the hydrogenation reaction.

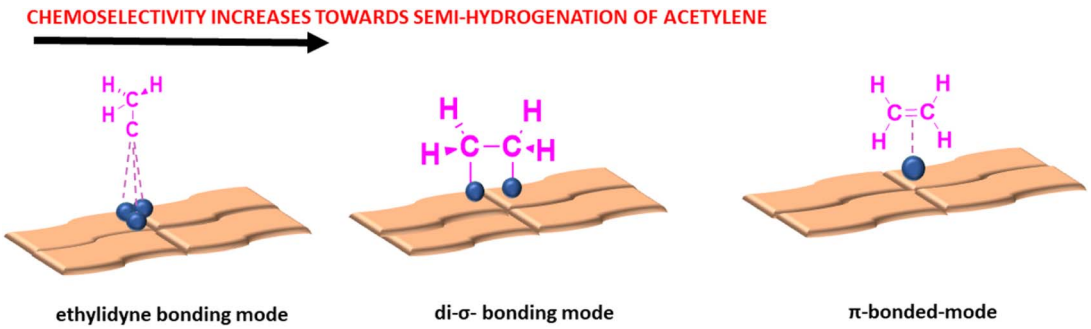

Fig. 20 An illustration of increasing chemoselectivity for semi-hydrogenation of acetylene on SACs.

molecules by controlling the configuration of adsorption sites and promoting the formation of low-energy transition states. Thus, the construction of more sterically hindered sites around the active metal centers results in better performance of SACs than their nanoparticle counterparts.[141,149]

4.3 Oxidation reactions

Most oxidation reactions require harsh reaction conditions like high temperature and pressure to give high yields. Poor chemoselectivity is a limiting factor for such organic transformations.[150,151] A strong metal–support interaction and the ability to activate oxidising species are the two most important factors for developing a highly selective catalyst for such reactions. The type of oxygen species adsorbed and activated on the surface of the catalyst depends on the surface properties like defects, vacancies and arrangement of the atoms on the surface of the catalyst. It is found that when Pt SAC is dispersed onto the surface of MgO nanosheets, it shows superior oxidation of toluene as compared to the MgO nanosheet alone. The introduction of SACs reduces the formation energy of oxygen vacancies (4.19 eV) on the catalyst, which acts as the active centers for the oxidative process. Their synthesized catalyst showed excellent activity in the presence of H_2O, which is contradictory to previous reports. DFT calculations suggested that this can be attributed to a lowered activation energy barrier for H_2O as compared to O_2 on Pt_1/MgO nanosheets.[152] Selective oxidation of benzene to phenol is a crucial chemical transformation for the production of resins, bisphenol, and nylon, but the traditional cumene process involves very harsh reaction conditions and also results in low yields while causing environmental pollution. Since modulation of the coordination environment of SACs with different heteroatoms like C, N and O results in unique geometrical and electronic structures, it is found that the Fe–N_4 coordination environment gives the best conversion and selectivity as compared to the Fe–N_3C_1 and Fe–N_2C_2 coordination environment for benzene oxidation to phenol. DFT calculations and temperature-programmed desorption (TPD) measurements revealed that the increase in the Fe–N coordination number results in more facilitated adsorption and activation of O_2 molecules and also enhances hydrophilicity of the catalyst, which promotes better interaction with the substrates of the reaction.[153] A recent microkinetic model-based study conducted to understand the influence of coordination of different transition metals with four N atoms revealed that such a microenvironment is necessary for C–H bond activation of benzene and O–H bond weakening of phenol, which ultimately results in better conversions.[154] While the introduction of carbon into the coordination environment of SACs is found to degrade the percentage conversion, the introduction of heteroatoms like oxygen along with nitrogen for coordinating SACs is surprisingly found to enhance such conversions from 78.4% to 98.1% of phenol. This can be attributed to the synergy of high electrophilicity of O and more number of unoccupied 3d-orbital present on the partially oxidized central metal, which helps with easy excitation of electrons and hence yields highly selective outcomes at a low concentration of H_2O_2.[155] Similar observations are also made by W. Chen and co-workers where dual-coordinated Cu_1–N_3O_1 moiety does not require the H_2O_2 activation step due to which the activation energy barrier for the oxidation reaction is significantly lowered and hence results in higher turn-over frequency.[156]

4.4 C–C cross coupling reaction

Suzuki–Miyaura cross-coupling reaction is a well-known reaction for C–C bond formation for organic synthesis of various bioactive molecules and natural products. Moreover, they are used for the production of a large number of materials, such as molecular wires, liquid crystals, and conducting polymers. Conventionally, Pd-phosphine complexes are used for cross-coupling reactions. The phosphine ligands help the interconversion of oxidation states between Pd(0) and Pd(II) by reversibly dissociating from Pd. However, the high moisture and air sensitivity of the phosphorus ligand pose difficulty in the recovery and reuse of the catalyst and they often get oxidized to phosphine oxide. The high cost and toxic nature of palladium remain a challenge for their large-scale production in industries. Therefore, the development of a non-toxic, environmentally benign, cost-effective and highly efficient alternative to the Pd-based catalyst is becoming extremely popular among the research community. In the C–C cross coupling reaction, the valence state of the metal changes dynamically during the oxidative addition and reductive elimination pathways. This dynamic change of the valence state of the metal at the active center becomes a challenge during the development of a suitable catalyst. SACs have been found to be more chemo-selective

as compared to nanoparticles because of their restricted adsorption modes and high atom utilization; however, leaching or deactivation of the single metal atoms from the support and insufficient activation of the substrate are some of the challenges that need to be addressed.[113,157,158] There have been few works where Pd-based SACs have been used as an efficient catalyst for catalyzing the Suzuki–Miyaura reaction.[159,160] The dependence of the reaction on phosphine ligands puts forward a limitation for the reaction because of the high cost and complicated nature of the procedure. So, the need to lift this limitation and the goal of efficient reaction at room temperature led to the development of an atomically dispersed palladium catalyst supported onto oxides and bimetallic oxides like ZnO–ZrO_2.[160,161] J. Du and co-workers adopted the strategy of using MOF-derived N–C carriers as supports for stabilizing atomically dispersed Pd onto the surface. The unique structure of MOF-derived SACs proved to show high catalytic activity for a longer duration without much reduction in catalytic performance. They doped ZrO_2 in UiO-66-NH_2 to anchor the Pd single atoms and developed N-doped carbon supports for holding the Pd single metal atoms in place. Their results indicated that uncoordinated functional groups are extremely important for binding and stabilizing single metal atoms. The absence of these uncoordinated functional groups often leads to aggregation of single atoms into nanoparticles, which is found to cause a reduction in their catalytic activity. The ZrO_2 doping into the –NH_2 functionalized MOF framework (UiO-66-NH_2) has been shown to increase the Pd loading from 0.15% to 0.27%, which points towards the importance of doping of metal oxides with functionalized MOF frameworks. Fig. 21 depicts the catalytic scheme in which electron transfer from Zr ions to Pd leads to the generation of electron-rich Pd, which helps to make the oxidative addition process faster and easier.[160]

The flat surface and open active sites of the supports often lead to poor interaction of the active sites with the reactant molecules. The addition of an organic monolayer can modulate the microenvironment of Pd atoms and improve its extent of interaction with the substrate, similar to ligands of a homogeneous catalyst. Fig. 22 shows the probable π-stacking between the aromatic catechol (CTE) ring and reactants on the surface of CeO_2, which stabilizes the transition state and hence accelerates the reaction. However, the addition of bulkier organic molecules results in the blockage of Pd active sites. Thus, using catechol rings provides better π-stacking interaction, which compensates for the steric hindrance.[162–164]

Excellent conversion to biphenyls is also observed in the case of various carbon-supported Pd ADMCs, attributing to their abundant anchoring sites, larger specific surface area and 3D-structure of the anchoring sites for active metal centers.[100,165,166] However, the design and development of atomically dispersed metals other than Pd have become more desirable, considering the drawbacks associated with a Pd-based catalyst.

A major portion of the sunlight is composed of visible light. Photocatalytic organic reactions in the visible region have become a breakthrough solution for the growing energy demands and provide a greener and more sustainable route for the generation of value-added products.[167–169] Recently, Cu SACs embedded into the intra and interlayers of the carbon nitride (CN) framework, as shown in Fig. 23, have been proven to improve the catalytic behavior of Pd-based catalysts for photocatalytic Suzuki–Miyaura cross-coupling reaction. These incorporated metal atoms act as mediators for electrons to reach the Pd species at the catalyst surface so that electron-rich Pd species responsible for catalyzing the Suzuki–Miyaura cross-coupling reaction could be formed easily. Such intercalation of the transition metal single atoms in between the layers of 2D support assists the noble metals on the surface of the support by promoting faster charge transfer to the LUMO of the aryl halides, thereby enhancing the rate-determining step of the C–C

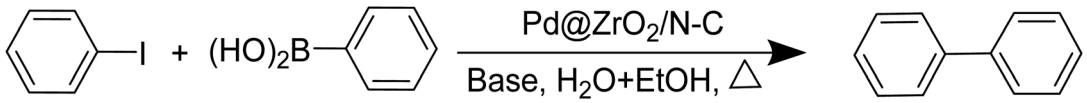

Fig. 21 A schematic representation of the Suzuki–Miyaura cross coupling reaction catalyzed by the Pd@ZrO_2/N–C SAC.

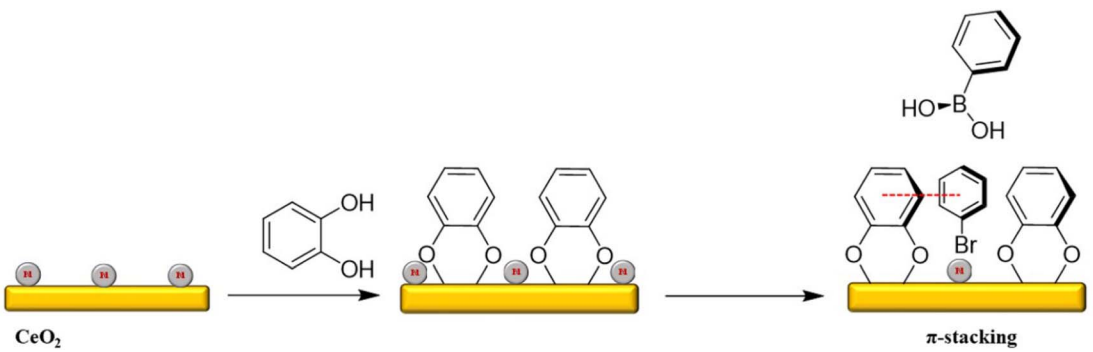

Fig. 22 A schematic representation of CTE modification of Pd/CeO_2 and subsequent π-stacking between CTE and substrates.

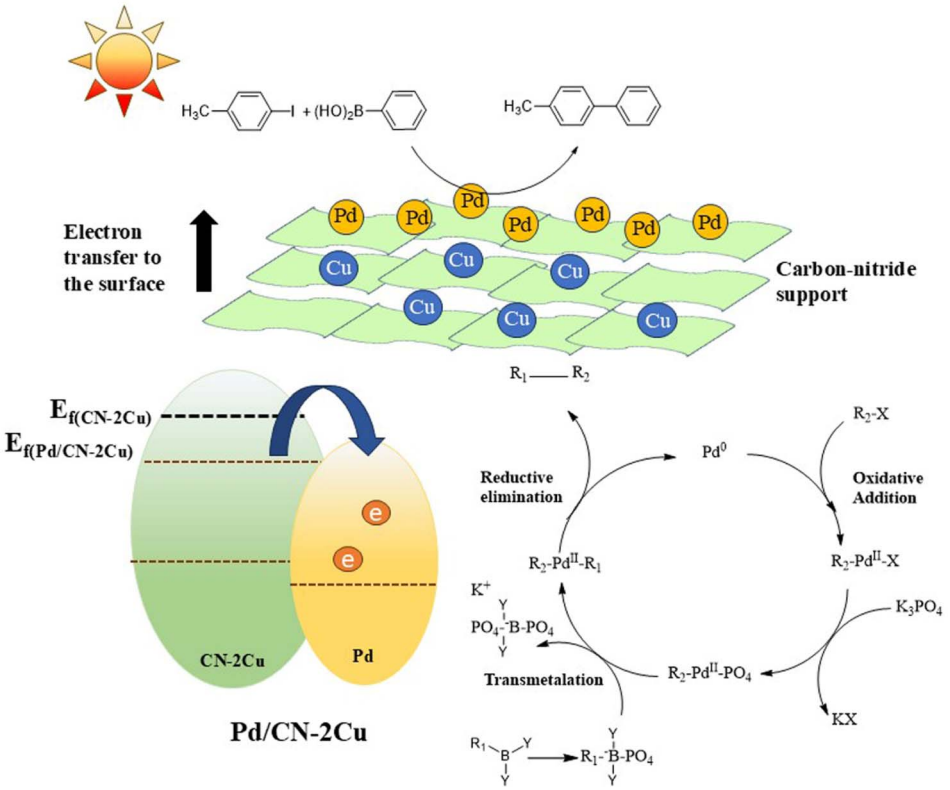

Fig. 23 An illustration of the impact of Cu SAC incorporation into intra/interlayers of the carbon–nitride support on bandgap tuning and catalytic cycle of the photocatalytic Suzuki–Miyaura cross coupling reaction.

coupling reactions.[125] Thus, a highly efficient support must not only stabilize the single atoms but should also be modified in such a way that maximum charges reach the catalyst surface for faster oxidative addition processes in C–C cross-coupling reactions.[160,161,167–169]

Since the Suzuki–Miyaura cross-coupling reaction proceeds through a series of elementary steps, enough coordination sites of the catalyst are required for the utmost efficiency of the photocatalytic process. So, supports that can provide reversible coordination sites seem extremely beneficial for such reactions. The microstructure of 2D g-C_3N_4 and its N-coordination sites give rise to weak bonds between the active metal and coordination sites of the support, which can reversibly bind with substrates during reactions. Such structures of the supported SACs resemble a homogeneous system, thereby resulting in better efficiency of the photocatalyst. Moreover, ligand-to-metal charge transfer (LMCT) between the active metal and the organic support and intrinsic HOMO–LUMO charge transfer in the organic support results in better charge separation, which ultimately gives rise to a superior photocatalytic behaviour.[170,171] ADMCs show excellent catalytic behavior even for other cross-coupling like Sonogashira, Ullman, and alcohol coupling.[170] Au alloyed SAAs like Au–Pd and Au–Cu have shown high catalytic conversions for the Ullmann and Sonogashira type of coupling. The decreasing active metal-to-host metal ratio increases the separation between the active centers, resulting in a unique coordination environment and more coordination sites for substrates. A comparison based on the exponential correlation curve of TON revealed that low-coordinated corner and edge Pd atoms of Au–Pd are the active centers for the Sonogashira coupling reaction. Moreover, the synergic effect and close proximity of the two different metals often result in unique binding modes, which help with the activation and subsequent coupling of various organic molecules.[172,173] The coordination of Pd single atoms to the TiO_2 surface through four oxygen atoms is energetically found to be favourable. Such a coordination environment leads to effortless adsorption and cleavage of the C–I bond of iodobenzene on Pd atoms and ensuing C–H bond activation on TiO_2 oxygen. The as-obtained phenyl and phenylacetylenyl then couple together due to their close proximity.[174] Apart from C–C cross coupling reactions, N–N bond formation is another crucial industrially important organic transformation with potential benefits for the dye, pharmaceutical and food additive industries. Commonly, such reactions proceed through oxidative coupling of the substrates to form azo dyes. However, such mechanistic pathways often require high temperatures and toxic oxidants, which often lead to uncontrolled reactions, thus affecting the overall selectivity and efficiency of reactions. However, the high efficiency of SACs for hydrogenation reactions helps in proceeding with the reaction through a hydrogenative coupling pathway, which seems more sustainable and results in higher product yields with better selectivity.[175–177]

4.5 Click reaction

The very well-known click reaction is a class of simple and highly convenient reactions that fits best as a green transformation. This reaction results in the formation of triazoles, which are crucial for the synthesis of drugs, pesticides, natural compounds, and other valuable materials.[178,179] Various homogeneous as well as heterogeneous Cu(I) based catalysts have already been used as effective catalysts for this reaction. However, they often suffer from rapid catalyst deactivation, product contamination and reduced selectivity, even though their activity is very high. Moreover, Cu is cytotoxic in nature and is incompatible with living systems, so researchers are switching to Cu-free catalysts for click reactions. But, none can match the high activity of Cu(I) catalysts.[178] Therefore, to overcome these drawbacks of traditional homogeneous and heterogeneous catalysts, a Cu-based SAC supported on g-C_3N_4 was synthesized. The development of such SACs helps to enhance selectivity while reaping maximum benefits of the high activity of Cu(I) species at their lowest possible metal content. Fig. 24 illustrates various anchoring sites on the surface of a mesoporous polymeric graphitic carbon nitride for Cu single atoms. It was concluded that a mixture of sites (a–e) is responsible for anchoring the Cu single atoms.[179]

Their synthesized catalyst exceeds other Cu(I) nanoparticles in terms of performance by avoiding leaching of the catalyst, which may be due to the adsorption of the Cu single atoms into the heptazinic pores of the g-C_3N_4. They found that the synthesized catalyst showed better activity over all the other homogeneous as well as heterogeneous catalysts with a turnover frequency of 189 h^{-1}. This tremendous catalytic activity of their synthesized catalyst is because of the atomic dispersion of Cu over the surface of mesoporous g-C_3N_4, which makes a large number of unsaturated coordination sites available for the substrates to attack.[179] P. Ren and co-workers also developed a Cu SAC supported on N-doped porous carbon, which also showed excellent selectivity towards the targeted 1,4-disubstituted 1,2,3-triazole by making use of a large number of alkynes and azides under mild reaction conditions in a cost-effective and environmentally benign way. Even after several successive cycles, they spotted no leaching of the catalyst, which suggested that their synthesized catalyst showed excellent stability and catalytic properties.[178] Fig. 25 clearly illustrates that surface active metals are extremely important for efficiently catalyzing the reaction. In homogeneous catalysts, catalytically active Cu(I) species might also be trapped inside the bulk of the catalyst because of which the catalytically active species cannot be efficiently approached by the substrate. The mesoporous structures of support materials with lone pairs containing atoms on their surfaces act as Lewis acid sites for generating abundant Cu(I) SACs on the exposed surfaces of the catalyst, resulting in greater interaction of the substrate with the Cu(I) sites for rapid formation of the intermediate, thereby enhancing the catalytic rates. Organic supports with a high degree of porosity are often chosen for stabilizing the single atoms for most click

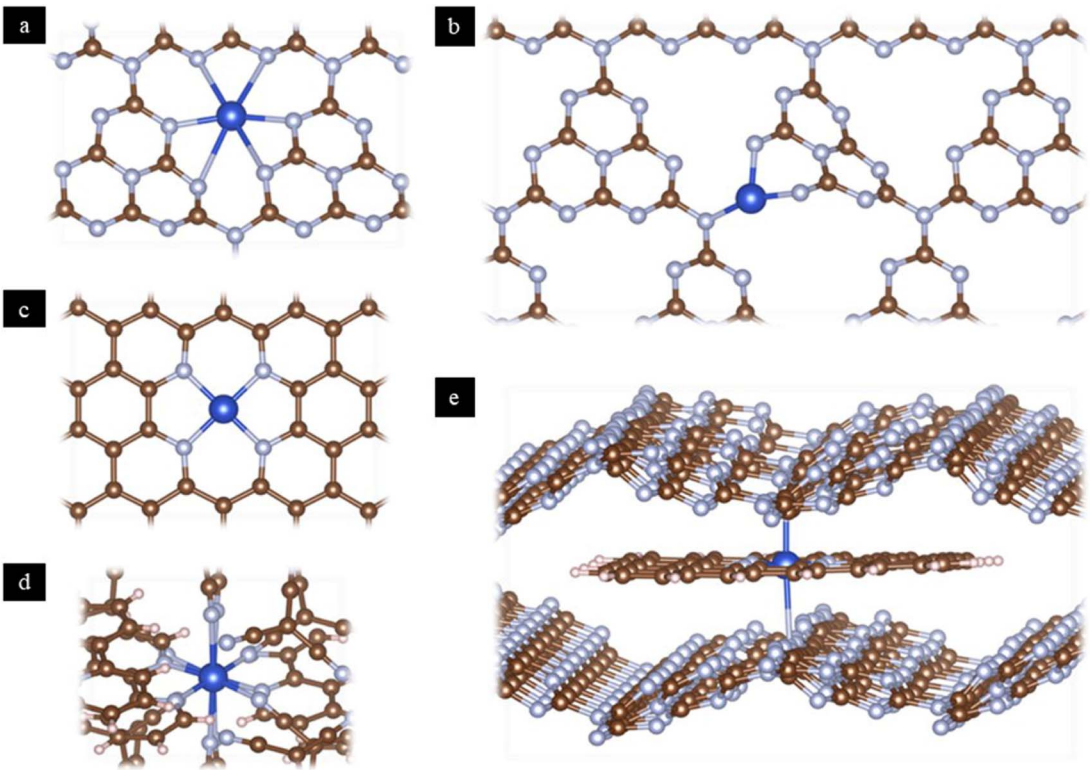

Fig. 24 An illustration of the structural features of Cu adsorbed in the heptazinic pore of mpgC_3N_4 (a) C substituted by Cu in mpgC_3N_4 (b) dicarbon vacancy in N-doped graphene hosted by Cu (c), octahedral complex $[Cu(bpy)(tcm)_4]^{2+}$ (d) and sandwich-like arrangement of Cu-doped N-graphene intercalated in mpgC_3N_4 (e). Reproduced with permission from ref. 179. Copyright 2022, *ACS Catal.*

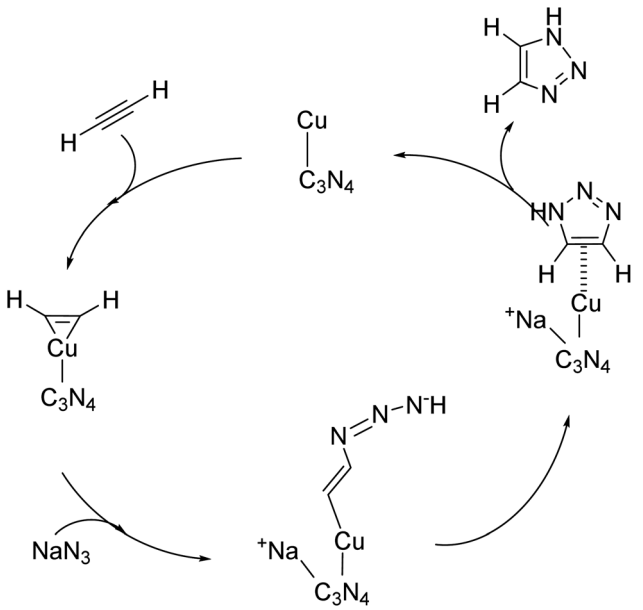

Fig. 25 A schematic representation of the proposed catalytic cycle for triazole formation over supported Cu SAC. Reproduced with permission from ref. 179. Copyright (2022), *ACS Catal.*

reactions because their mesoporous nature exposes a larger number of active sites, which causes a better charge transfer and results in better adsorption of the substrates onto the active site. Moreover, unlike other Cu nanoparticle-based catalysts, SACs anchored onto such mesoporous supports provide a larger surface area and stronger metal–support interaction, due to which there is minimum loss of active sites over time, resulting in higher durability as well as higher selectivity of the catalyst.[178,179]

Similarly, some recent works on the azide–alkyne cycloaddition reaction catalyzed by Cu-based SAC showed positive outcomes and amazing sustainable results.[180] Modulation of the microenvironment of Cu SACs gives rise to stronger metal–support interactions and more suitable geometry for interaction with substrates. Cu(II) SACs bonded to the support through both N and O give better conversions than their N-bonded counterparts. This might be because of the greater electronegativity of O as compared to N, which makes the active metal center more electrophilic in nature, resulting in accelerated rates. Moreover, the comparatively stronger M–O bonds prevent the leaching of the catalyst by preventing their aggregation.[112] Noble metals like Ru, Au, Ag and Ir are proven to be good candidates for catalyzing the azide–alkyne cycloaddition, among which Ru is more widely explored.[159] The uniqueness of the Ru-based homogeneous catalyst lies in the fact that it gives rise to regioselective product 1,5-disubstituted 1,2,3-triazoles, unlike the traditional CuAAC-catalyst that results in both 1,4 and 1,5- disubstituted regioisomers at elevated temperatures.[181,182] But, the homogeneous nature of the catalyst and bulky nature of the ligand hampers the recyclability of the catalyst, and at the same time, provides steric hindrance in the reaction. Moreover, the potential of SACs composed of metals other than Cu(I) has not been explored well till now.

According to Y. Li and co-workers, it was concluded that a metal-to-ligand charge transfer (MLCT) occurs when metals like Pt and Cu are anchored onto the surface of g-C_3N_4. Such charge transfer processes give rise to a narrow bandgap as compared to traditional HOMO to LUMO charge transfer processes, thereby causing absorption at a longer wavelength by preventing rapid charge recombination. The highly unsaturated nature of isolated single atoms not only helps with the better adsorption of molecules but can also act as the center of light harvesting at the same time. Due to the flexible nature of the SAC, it can also be intercalated between the layers of organic supports, which can act as a medium for transferring the

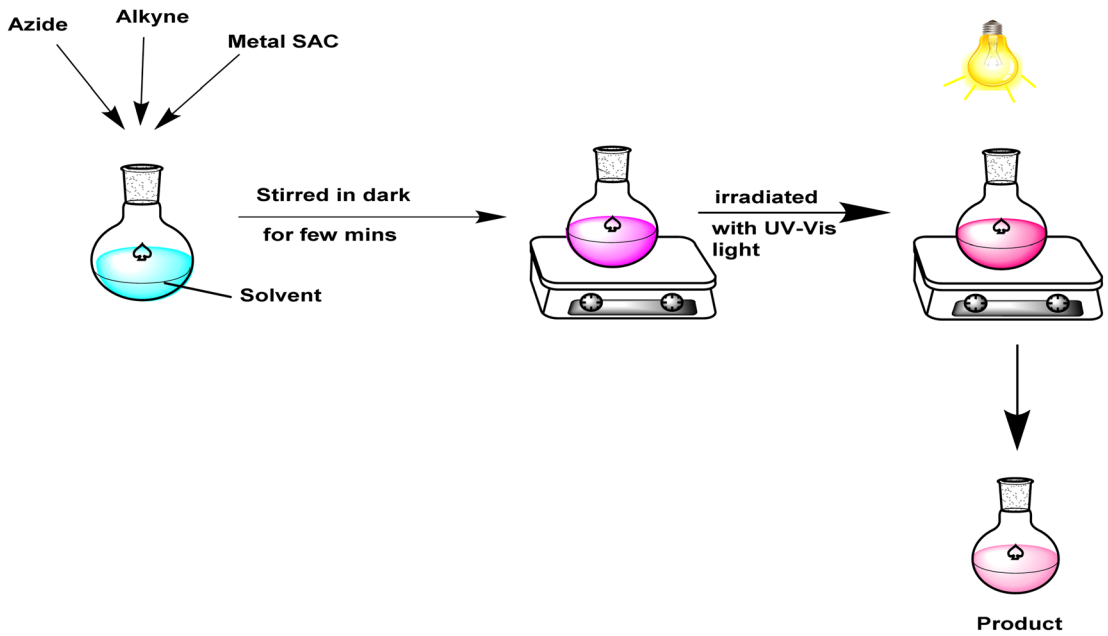

Fig. 26 A schematic representation of the photocatalytic azide–alkyne cycloaddition reaction.

Table 2 A list of different SACs used for the C–C cross coupling reaction, biomass-conversion and azide–alkyne cycloaddition click reaction

Organic reaction	Reactant	Product	Catalyst used	Condition	Yield/conversion/selectivity (%)	Reference
C–C cross coupling reaction	Iodobenzene, phenylboronic acid	Biphenyl	$Pd@ZrO_2/N–C$	Thermal	99	160
	Bromobenzene, *p*-tolyl boronic acid	4-Methylbiphenyl	Pd/CeO_2	Room temperature	89 ± 6	162
	4-Iodotoluene, phenylboronic acid	4-Phenyltoluene	Pd/CN–*x*Cu	Photocatalytic	98	168
Hydrogenation reaction	Crotonaldehyde	Crotyl alcohol	Rh_1/MoS_2	Thermal	100	141
Oxidation reaction	Acetylene	Ethylene	Pd_1/C_3N_4	Thermal	99, 83	148
	Ethylbenzene	Acetophenone	Co SACs	Thermal	97	107
Biomass-conversion	Benzene	Phenol	Cu_1/NOC	Thermal	70.9, 94	156
	Levulinic acid	γ-valerolactone	$Ru_1Co@N–C–x$	Thermal	98	117
	2-Phenoxy-1-phenylethanol	Cα–Cβ cleavage products	Pt_1/N-CNTs	Electrocatalytic	81	119
	5-Hydromethylfurfural	2,5-Dimethylfuran	Pt_1/Co SAA	Thermal	100	2
	5-Hydromethylfurfural	2,5-Furandicarboxylic acid	Ru_1/CoO_x	Electrocatalytic	76.5	120
Click reaction	Benzyl bromide, DMF, phenylacetylene	1-Benzyl-4-phenyl-1*H*-1,2,3-triazole	saCu-2 @ $mpgC_3N_4$	Thermal	45	179
	Azide, alkyne	Substituted triazoles	Cu_1/NC-800	Thermal	>99	178

maximum number of photogenerated charges to the surface for catalyzing the reaction.[183–187] Considering all these positive aspects of SACs, they can also be utilized for photocatalytic click reactions (Fig. 26); however, such investigations are still in their infancy stage. Table 2 lists the different types of SACs that are highly efficient for various industrially important organic reactions. This table will help identify which type of SACs are beneficial for a specific reaction.

The production of bio-based azides is found to be extremely beneficial for sustainability as they are derived from lingocellulosic biomass. These bio-based azides are useful for the bioconjugation of biomolecules, which is an important tool for developing pharmaceutical industries. However, their use is often limited to academia because of their hazardous nature, which hinders their scale-up in industries. They can be easily derived from readily available monosaccharides and disaccharides in a pure diastereomeric form, which aids their practical utility for Cu-based click reactions.[188,189] Lignocellulosic biomass-based building blocks are also beneficial for sustainable thiol–ene clicking reactions, which help build covalent interaction between ene functionalities beneficial for polymer synthesis. Conventional methods use large quantities of Cu(II) salts with reducing tendencies but often come with the disadvantage of undesirable side reactions, which might alter the structures of biomolecules during bioconjugation.[189] However, SACs offer catalytic poisoning effects due to their ability to alter binding modes, which makes them potential candidates for catalyzing click reactions of biomass-based substrates. Moreover, compared to the nanoparticles, the isolated environment and high chemoselectivity of the SACs can potentially promote the orthogonality of the reactions, thereby promoting one-pot click reactions.[141,144,190] Oxidation-induced click reactions have also taken the central stage in recent years due to their tremendous benefits but oxidative processes often lead to the generation of highly reactive functional groups.[190] So, reaction kinetics need to be controlled to eliminate the possibility of side reactions, which can be achieved by downsizing the nanoparticles to SACs and controlling their distribution.

5. Conclusion and future perspective

The atomic dispersion of active metal species on a suitable support surface promises maximum atom utilization at the lowest metal content by providing maximum unsaturated sites. However, developing highly efficient SACs requires precise control over the metal loading. It is not only the high metal loading that matters while determining the efficiency of the catalyst but also the actual number of catalytically exposed active sites whose density needs to be higher for maximum activity. The isolation of active sites provides an opportunity to modulate the local environment of the active metal species, leading to an ensemble effect, which can alternate the reaction pathways, thus resulting in more energy-efficient reactions. With the growing energy crisis, sustainable approaches towards various industrially important organic transformations like biomass conversion, hydrogenation, oxidation, C–C coupling reaction and click chemistry have become

a cause of concern for the research community. It is observed that selective hydrogenation is a crucial step for biomass conversion as well as most other organic transformations. The isolation of the active sites gives rise to a poisoning effect, which prevents undesirable side reactions, thus enhancing selectivity. Moreover, the synergy of H_2 molecule activation followed by its spillover and unique η^1 mode of adsorption on SACs helps to achieve such energetically demanding selective hydrogenation. A strong metal–support interaction unique to SACs is also another factor responsible for their better performance than other supported nanoparticles. It was found that defect and vacancy-rich support is most ideal for stabilizing selective SACs. Synthesis of more sterically hindered structures surrounding the active metal center prevents further adsorption of unwanted intermediates, thus preventing side reactions. It is observed that the incorporation of SACs on various kinds of supports decreases the activation energy for the formation of oxygen vacancies, which is the governing factor for deciding the type of oxygen species adsorbed and activated on the surface of the catalyst for oxidative processes. The neighbouring groups and coordination number of the active metal species can alter the reaction kinetics, as it is evident from the fact that the introduction of carbon into the coordination environment of SACs is found to degrade the percentage conversion, whereas the introduction of heteroatoms like oxygen along with nitrogen for coordinating SACs is surprisingly found to enhance selective oxidation processes. C–C bond and C–N bond construction are extremely important for the synthesis of various compounds like agrochemicals, pharmaceuticals, and other special chemicals. Recently, Pd SACs have been extensively used as catalysts for the Suzuki–Miyaura coupling reaction. C–C coupling reactions require a large number of unsaturated reversible coordination sites, which are effectively provided by SACs. This results in their superior performance as compared to other catalysts. But, due to the high cost of Pd, developing transition metal-based SACs is more desirable. Although Cu SACs have been developed as a co-catalyst for such conversions, they have not been able to replace Pd-based SACs. Apart from C–C cross coupling reactions, N–N bond formation is another crucial industrially important organic transformation that usually requires high temperature and toxic oxidants, often leading to uncontrolled reactions. However, the high efficiency of SACs for hydrogenation reactions helps proceed with the reaction through a hydrogenative coupling pathway, which seems more sustainable and results in higher product yields with better selectivity. Carbon supports with a high degree of porosity are often chosen for anchoring Cu SACs for most of the azide–alkyne cycloaddition reactions as they expose a larger number of active sites, which causes a better charge transfer and results in better adsorption of the substrates onto the active site. Such mesoporous support-based SACs provide a larger surface area and stronger metal–support interaction that leads to minimum loss of active sites over time, thus resulting in higher durability as well as higher selectivity of the catalyst. Lignocellulosic biomass-based building blocks are beneficial for sustainable thiol–ene clicking reactions. Conventional catalysts often suffer from undesirable side reactions that might alter the structures of biomolecules during bioconjugation. The isolated nature of SACs and the ability to alter binding modes can enhance the chemoselectivity of the reaction, which can potentially promote the orthogonality of the reactions, thereby promoting one-pot click reactions. Oxidation-induced click reactions have also taken the central stage in recent years due to their tremendous benefits but oxidative processes often lead to the generation of highly reactive functional groups. So, reaction kinetics need to be controlled to eliminate the possibility of side reactions, which can be achieved by downsizing the nanoparticles to SACs and controlling their distribution. When the nanoparticles are downsized to single atoms, the quantum confinement effect gives rise to a unique HOMO–LUMO energy gap of SACs, proving it to be an outstanding photocatalyst. The perfect combination of unsaturated sites, unique electronic properties and precise modulation of the local environment seems to help develop highly selective photocatalysts for various sustainable organic transformations. The piezoelectric behavior of catalysts has been explored for photocatalytic activation of small molecules like H_2O, O_2 *etc.* However, such strategies can be extended to activate larger organic molecules by using the extraordinary potentials of SACs. Supports like MOF can behave as photoswitches because of their flexible pores. Such photoresponsivity of MOF can be used for photocatalyzing the organic molecules if highly active metal nodes are incorporated into it as single atoms. It is clearly evident that, most often, highly complicated procedures are adopted to develop SACs. Strategies like MOF-derived SACs involve a very cumbersome process. So, researchers should consider simpler methods for the preparation of SACs so that any additional physical and chemical processes can be avoided. There is a huge scope for surface engineering of support, which determines the number of catalytically active single atoms anchored onto its surface. By manipulating the morphology of the support material, one can control the number of exposed planes responsible for anchoring the maximum dispersion of single atoms, consequently yielding highly efficient SACs. New strategies need to be introduced to enhance the stability and lifetime of SACs. The upscaling and practical utility of the catalyst is still a huge challenge to overcome.

Abbreviations

SAC:	Single atom catalyst
ADMC:	Atomically dispersed metal catalyst
EF:	Formation energy
MOF:	Metal–organic framework
CTE:	Catechol
LMCT:	Ligand to metal charge transfer
HOMO:	Highest occupied molecular orbital
LUMO:	Lowest unoccupied molecular orbital
CN:	Carbon nitride
LA:	Levulinic acid
GVL:	γ-Valerolactone
HMF:	5-Hydroxymethylfurfural
DFF:	2,5-Diformylfuran
FDCA:	2,5-Furandicarboxylic acid
TPD:	Temperature programmed desorption

Data availability

The data supporting this article have been included as part of the manuscript. No primary research results, software or code have been included and no new data were generated or analysed as part of this review.

Conflicts of interest

There is no conflict of interest in this report and the authors declare no competing financial interest.

Acknowledgements

D. R is grateful to DST, India, for DST-INSPIRE research fellowship. We sincerely thank DST for financial support under the DST-PURSE project (SR/PURSE/2022/143 (C)) and DST-FIST project (SR/FST/CS-I/2020/152). The authors are thankful to Dibrugarh University for providing the infrastructure.

References

1 Y. Han, J. Dai, R. Xu, W. Ai, L. Zheng, Y. Wang, W. Yan, W. Chen, J. Luo, Q. Liu, D. Wang and Y. Li, *ACS Catal.*, 2021, **11**, 2669–2675.
2 T. Gan, Y. Liu, Q. He, H. Zhang, X. He and H. Ji, *ACS Sustain. Chem. Eng.*, 2020, **8**, 8692–8699.
3 C. Li, J. Li, L. Qin, P. Yang and D. G. Vlachos, *ACS Catal.*, 2021, **11**, 11336–11359.
4 P. K. Prajapati, S. Saini and S. L. Jain, *J. Mater. Chem. A*, 2020, **8**, 5246–5254.
5 M. Chetia, A. A. Ali, D. Bhuyan, L. Saikia and D. Sarma, *New J. Chem.*, 2015, **39**, 5902–5907.
6 Z. H. Xue, D. Luan, H. Zhang and X. W. D. Lou, *Joule*, 2022, **6**, 92–133.
7 P. V. Markov, G. O. Bragina, N. S. Smirnova, G. N. Baeva, I. S. Mashkovsky, E. Y. Gerasimov, A. V. Bukhtiyarov, Y. V. Zubavichus and A. Y. Stakheev, *Inorganics*, 2023, **11**, 150.
8 M. R. I. Sardar, F. Hasan, M. J. Alam, I. H. Nadim and M. Mahmud, *Appl. Organomet. Chem.*, 2023, **3**, 108–122.
9 M. S. Hasan, M. R. Sardar, A. Shafin, M. S. Rahman, M. Mahmud and M. M. Hossen, *J. Chem. Rev.*, 2023, **5**, 56–82.
10 Q. Wang, D. Zhang, Y. Chen, W. F. Fu and X. J. Lv, *ACS Sustain. Chem. Eng.*, 2019, **7**, 6430–6443.
11 C. Gao, J. Low, R. Long, T. Kong, J. Zhu and Y. Xiong, *Chem. Rev.*, 2020, **120**, 12175–12216.
12 G. Giannakakis, S. Mitchell and J. Pérez-Ramírez, *Trends Chem.*, 2022, **4**, 264–276.
13 Y. Wang, X. Cui, J. Zhang, J. Qiao, H. Huang, J. Shi and G. Wang, *Prog. Mater. Sci.*, 2022, **128**, 100964.
14 D. D. Ma and Q. L. Zhu, *Coord. Chem. Rev.*, 2020, **422**, 213483.
15 R. T. Hannagan, G. Giannakakis, M. Flytzani-Stephanopoulos and E. C. H. Sykes, *Chem. Rev.*, 2020, **120**, 12044–12088.
16 Y. Wang, X. Huang and Z. Wei, *Chin. J. Catal.*, 2021, **42**, 1269–1286.
17 S. Kment, A. Bakandritsos, I. Tantis, H. Kmentová, Y. Zuo, O. Henrotte, A. Naldoni, M. Otyepka, R. S. Varma and R. Zbořil, *Chem. Rev.*, 2024, **124**, 11767–11847.
18 B. B. Xu, X. B. Fu, X. M. You, E. Zhao, F. F. Li, Z. Chen, Y. X. Li, X. L. Wang and Y. F. Yao, *ACS Catal.*, 2022, **12**, 6958–6967.
19 B. Xia, Y. Zhang, J. Ran, M. Jaroniec and S. Z. Qiao, *ACS Cent. Sci.*, 2021, **7**, 39–54.
20 M. K. Samantaray, V. D'Elia, E. Pump, L. Falivene, M. Harb, S. Ould Chikh, L. Cavallo and J. M. Basset, *Chem. Rev.*, 2019, **120**, 734–813.
21 D. Liu, Q. He, S. Ding and L. Song, *Adv. Energy Mater.*, 2020, **10**, 2001482.
22 X. Y. Wu, Z. Tang, X. Zhao, X. Luo, S. J. Pennycook and S. L. Wang, *J. Energy Chem.*, 2021, **61**, 195–202.
23 C. Qin, Q. Guo, J. Guo and P. Chen, *Chem.–Asian J.*, 2021, **16**, 1225–1228.
24 G. Liu, Y. Huang, H. Lv, H. Wang, Y. Zeng, M. Yuan, Q. Meng and C. Wang, *Appl. Catal., B*, 2021, **284**, 119683.
25 H. Niu, X. Wan, X. Wang, C. Shao, J. Robertson, Z. Zhang and Y. Guo, *ACS Sustain. Chem. Eng.*, 2021, **9**, 3590–3599.
26 S. Guo, Y. Zhao, C. Wang, H. Jiang and G. J. Cheng, *ACS Appl. Mater. Interfaces*, 2020, **12**, 26068–26075.
27 X. Xie, L. Shang, X. Xiong, R. Shi and T. Zhang, *Adv. Energy Mater.*, 2022, **12**, 2102688.
28 X. Li, P. Shen, Y. Luo, Y. Li, Y. Guo, H. Zhang and K. Chu, *Angew. Chem.*, 2022, **134**, e202205923.
29 S. Luo, L. Zhang, Y. Liao, L. Li, Q. Yang, X. Wu, X. Wu, D. He, C. He, W. Chen, Q. Wu, M. Li, E. J. M. Hensen and Z. Quan, *Adv. Mater.*, 2021, **33**, 2008508.
30 R. Lang, X. Du, Y. Huang, X. Jiang, Q. Zhang, Y. Guo, K. Liu, B. Qiao, A. Wang and T. Zhang, *Chem. Rev.*, 2020, **120**, 11986–12043.
31 B. H. Lee, S. Park, M. Kim, A. K. Sinha, S. C. Lee, E. Jung, W. J. Chang, K. S. Lee, J. H. Kim, S. P. Cho, H. Kim, K. T. Nam and T. Hyeon, *Nat. Mater.*, 2019, **18**, 620–626.
32 P. Paydari, N. Manavizadeh, A. Hadi and J. Karamdel, *J. Sol-Gel Sci. Technol.*, 2023, **105**, 337–347.
33 B. Syal, P. Kumar and P. Gupta, *ACS Appl. Nano Mater.*, 2023, **6**, 4987–5041.
34 P. Li, X. Chen, Y. Li and J. W. Schwank, *Catal. Today*, 2019, **327**, 90–115.
35 Y. Zheng, Q. Wang, Q. Yang, S. Wang, J. M. Hulsey, S. Ding, S. Furukawa, M. Li, N. Yan and X. Ma, *ACS Catal.*, 2023, **13**, 7243–7255.
36 K. Razmgar, M. Altarawneh, I. Oluwoye and G. Senanayake, *Catal. Surv. Asia*, 2021, **25**, 27–47.
37 W. Z. Yu, W. W. Wang, S. Q. Li, X. P. Fu, X. Wang, K. Wu, R. Si, C. Ma, C. J. Jia and C. H. Yan, *J. Am. Chem. Soc.*, 2019, **141**, 17548–17557.
38 G. Righi, R. Magri and A. Selloni, *J. Phys. Chem. C*, 2019, **123**, 9875–9883.
39 H. Wang, C. Yue, J. Du, M. Pu and M. Lei, *J. Phys. Chem. C*, 2023, **127**, 16880–16890.

40 S. Tomar, B. S. Bhadoria, H. Jeong, J. H. Choi, S. C. Lee and S. Bhattacharjee, *J. Phys. Chem. C*, 2024, **128**, 8580–8589.
41 J. Xu, Y. Wang, K. Wang, M. Zhao, R. Zhang, W. Cui, L. Liu, M. S. Bootharaju, J. H. Kim, T. Hyeon, H. Zhang, Y. Wang, S. Song and X. Wang, *Angew. Chem., Int. Ed.*, 2023, **62**, e202302877.
42 P. Liu, Y. Zhao, R. Qin, S. Mo, G. Chen, L. Gu, D. M. Chevrier, P. Zhang, Q. Guo, D. Zang, B. Wu, G. Fu and N. Zheng, *Science*, 2016, **352**, 797–800.
43 H. Wei, K. Huang, D. Wang, R. Zhang, B. Ge, J. Ma, B. Wen, S. Zhang, Q. Li, M. Lei, C. Zhang, J. Irawan, L. M. Liu and H. Wu, *Nat. Commun.*, 2017, **8**, 1490.
44 H. Bi, L. X. Zhang, Y. Xing, P. Zhang, J. J. Chen, J. Yin and L. J. Bie, *Sens. Actuators, B*, 2021, **330**, 129374.
45 X. Chen, J. P. Cheng, Q. L. Shou, F. Liu and X. B. Zhang, *CrystEngComm*, 2012, **14**, 1271–1276.
46 Y. Sui, S. Liu, T. Li, Q. Liu, T. Jiang, Y. Guo and J. L. Luo, *J. Catal.*, 2017, **353**, 250–255.
47 R. Phul, V. Shrivastava, U. Farooq, M. Sardar, A. Kalam, A. G. Al-Sehemi and T. Ahmad, *Nano-Struct. Nano-Objects*, 2019, **19**, 100343.
48 Y. Zhang, J. Yang, R. Ge, J. Zhang, J. M. Cairney, Y. Li, M. Zhu, S. Li and W. Li, *Coord. Chem. Rev.*, 2022, **461**, 214493.
49 R. Ullah, *J. Chem. Rev.*, 2023, **5**, 466–476.
50 J. Ren, L. Tao, Z. Luo, J. Zeng and D. Yin, *ACS Appl. Eng. Mater.*, 2024, **2**, 988–999.
51 H. Wang, D. Xu, E. Guan, L. Wang, J. Zhang, C. Wang, S. Wang, H. Xu, X. Meng, B. Yang, B. C. Gates and F. S. Xiao, *ACS Catal.*, 2020, **10**, 6299–6308.
52 S. Dutta, *RSC Adv.*, 2012, **2**, 12575–12593.
53 W. J. Liu, X. Zhou, Y. Min, J. W. Huang, J. J. Chen, Y. Wu and H. Q. Yu, *Adv. Mater.*, 2024, **36**, 2305924.
54 Z. Xue, J. Yang, L. Ma, H. Li, L. Luo, K. Ji, Z. Li, X. Kong, M. Shao, L. Zheng, M. Xu and H. Duan, *ACS Catal.*, 2023, **14**, 249–261.
55 F. Lin, B. Cai, Z. Tang, G. Li, K. Wang, G. Chen and C. He, *ACS EST Eng.*, 2024, **4**, 1479–1491.
56 C. C. Hou, H. F. Wang, C. Li and Q. Xu, *Energy Environ. Sci.*, 2020, **13**, 1658–1693.
57 P. Xia, C. Wang, Q. He, Z. Ye and I. Sirés, *Chem. Eng. J.*, 2023, **452**, 139446.
58 Q. Zuo, T. Liu, C. Chen, Y. Ji, X. Gong, Y. Mai and Y. Zhou, *Angew. Chem., Int. Ed.*, 2019, **58**, 10198–10203.
59 Q. Yang, C. C. Yang, C. H. Lin and H. L. Jiang, *Angew. Chem., Int. Ed.*, 2019, **58**, 3511.
60 H. Wang, Y. Wang, Y. Li, X. Lan, B. Ali and T. Wang, *ACS Appl. Mater. Interfaces*, 2020, **12**, 34021–34031.
61 M. Li, C. Zhang, Y. Tang, Q. Chen, W. Li, Z. Han, S. Chen, C. Lv, Y. Yan, Y. Zhang, W. Zheng, P. Wang, X. Guo and W. Ding, *ACS Catal.*, 2022, **12**, 11960–11973.
62 M. Li, S. Chen, Q. Jiang, Q. Chen, X. Wang, Y. Yan, J. Liu, C. Lv, W. Ding and X. Guo, *ACS Catal.*, 2021, **11**, 3026–3039.
63 K. Sun, H. Shan, H. Neumann, G. P. Lu and M. Beller, *Nat. Commun.*, 2022, **13**, 1848.
64 B. Li, J. Kou, G. Zeng, J. Ma and Z. Dong, *ACS Catal.*, 2023, **13**, 16286–16299.
65 C. C. Hou, L. Zou, L. Sun, K. Zhang, Z. Liu, Y. Li, C. Li, R. Zou, J. Yu and Q. Xu, *Angew. Chem.*, 2020, **132**, 7454–7459.
66 R. Juarez, P. Concepción, A. Corma, V. Fornés and H. García, *Angew. Chem., Int. Ed.*, 2010, **49**, 1286–1290.
67 E. Tiburcio, R. Greco, M. Mon, J. Ballesteros-Soberanas, J. Ferrando-Soria, M. López-Haro, J. C. Hernández-Garrido, J. Oliver-Meseguer, C. Marini, M. Boronat, D. Armentano, A. Leyva-Pérez and E. Pardo, *J. Am. Chem. Soc.*, 2021, **143**, 2581–2592.
68 X. Ma, H. Liu, W. Yang, G. Mao, L. Zheng and H. L. Jiang, *J. Am. Chem. Soc.*, 2021, **143**, 12220–12229.
69 M. B. Gawande, P. Fornasiero and R. Zbořil, *ACS Catal.*, 2020, **10**, 2231–2259.
70 M. Xu, Y. Yu, G. Shi, P. Jian, X. Hou and E. Yuan, *ACS Appl. Nano Mater.*, 2024, **7**, 11952–11964.
71 J. Büker, X. Huang, J. Bitzer, W. Kleist, M. Muhler and B. Peng, *ACS Catal.*, 2021, **11**, 7863–7875.
72 H. Zhu, J. Zhao, Z. Yu, J. Li, C. Ma, H. Sun, Y. Wu and Q. Meng, *Ind. Eng. Chem. Res.*, 2023, **62**, 8253–8268.
73 Z. Chen, Y. Deng, G. Yang, Y. N. Zhu, Q. Zhang, Z. Liu, Y. Cao and F. Peng, *ACS Sustainable Chem. Eng.*, 2023, **11**, 5773–5781.
74 J. Li, S. Zhao, S. Z. Yang, S. Wang, H. Sun, B. Johannessen and S. Liu, *J. Mater. Chem. A*, 2021, **9**, 3029–3035.
75 J. Li, S. Zhao, L. Zhang, S. P. Jiang, S. Z. Yang, S. Wang, H. Sun, B. Johannessen and S. Liu, *Small*, 2021, **17**, 2004579.
76 M. T. Darby, E. C. H. Sykes, A. Michaelides and M. Stamatakis, *Top. Catal.*, 2018, **61**, 428–438.
77 W. Liu, H. Feng, Y. Yang, Y. Niu, L. Wang, P. Yin, S. Hong, B. Zhang, X. Zhang and M. Wei, *Nat. Commun.*, 2022, **13**, 3188.
78 M. B. Boucher, B. Zugic, G. Cladaras, J. Kammert, M. D. Marcinkowski, T. J. Lawton, E. Sykes, H. Charles and M. Flytzani-Stephanopoulos, *Phys. Chem. Chem. Phys.*, 2013, **15**, 12187–12196.
79 F. R. Lucci, J. Liu, M. D. Marcinkowski, M. Yang, L. F. Allard, M. Flytzani-Stephanopoulos and E. C. H. Sykes, *Nat. Commun.*, 2015, **6**, 8550.
80 G. X. Pei, X. Y. Liu, A. Wang, A. F. Lee, M. A. Isaacs, L. Li, X. Pan, X. Yang, X. Wang, Z. Tai, K. Wilson and T. Zhang, *ACS Catal.*, 2015, **5**, 3717–3725.
81 G. X. Pei, X. Y. Liu, X. Yang, L. Zhang, A. Wang, L. Li, H. Wang, X. Wang and T. Zhang, *ACS Catal.*, 2017, **7**, 1491–1500.
82 M. J. Islam, M. G. Mesa, A. Osatiashtiani, J. C. Manayil, M. A. Isaacs, M. J. Taylor, S. Tsatsos and G. Kyriakou, *Appl. Catal., B*, 2021, **299**, 120652.
83 R. Réocreux, P. L. Kress, R. T. Hannagan, V. Çınar, M. Stamatakis and E. C. H. Sykes, *J. Phys. Chem. Lett.*, 2020, **11**, 8751–8757.
84 G. Giannakakis, A. Trimpalis, J. Shan, Z. Qi, S. Cao, J. Liu, J. Ye, J. Biener and M. Flytzani-Stephanopoulos, *Top. Catal.*, 2018, **61**, 475–486.
85 T. Tang, Z. Wang and J. Guan, *Chin. J. Catal.*, 2022, **43**, 636–678.

86 Y. Mu, T. Wang, J. Zhang, C. Meng, Y. Zhang and Z. Kou, *Electrochem. Energy Rev.*, 2022, **5**, 1–42.
87 Z. Li, X. Dong, M. Zhang, L. Leng, W. Chen, J. H. Horton, J. Wang, Z. Li and W. Wu, *ACS Appl. Mater. Interfaces*, 2020, **12**, 57569–57577.
88 X. Tan, H. A. Tahini and S. C. Smith, *J. Phys. Chem. C*, 2021, **125**, 12628–12635.
89 J. He, N. Li, Z. G. Li, M. Zhong, Z. X. Fu, M. Liu, J. C. Yin, Z. Shen, W. Li, J. Zhang, Z. Chang and X. H. Bu, *Adv. Funct. Mater.*, 2021, **31**, 2103597.
90 W. Xiang, Y. Zhang, Y. Chen, C. J. Liu and X. Tu, *J. Mater. Chem. A*, 2020, **8**, 21526–21546.
91 A. Schneemann, V. Bon, I. Schwedler, I. Senkovska, S. Kaskel and R. A. Fischer, *Chem. Soc. Rev.*, 2014, **43**, 6062–6096.
92 A. Goulet-Hanssens, F. Eisenreich and S. Hecht, *Adv. Mater.*, 2020, **32**, 1905966.
93 W. Jiang, H. Zhu, J. Yang, B. Q. L. Low, W. Y. Wu, M. Chen, J. Ma, R. Long, J. Low, H. Zhu, J. Z. X. Heng, K. Y. Tang, C. H. Teng Chai, M. Lin, Q. Zhu, Y. W. Zhang, D. Chi, Z. Li, X. J. Loh, Y. Xiong and E. Ye, *Adv. Sci.*, 2023, **10**, 2303448.
94 Y. Li, J. Feng, Y. Zhao, J. Wang and C. Xu, *Appl. Surf. Sci.*, 2022, **599**, 153969.
95 S. Bai, F. Liu, B. Huang, F. Li, H. Lin, T. Wu, M. Sun, J. Wu, Q. Shao, Y. Xu and X. Huang, *Nat. Commun.*, 2020, **11**, 954.
96 L. Jurado, J. Esvan, L. A. Luque-Álvarez, L. F. Bobadilla, J. A. Odriozola, S. Posada-Pérez, A. Poater, A. Comas-Vives and M. R. Axet, *Catal. Sci. Technol.*, 2023, **13**, 1425–1436.
97 Y. Chen, R. Zhang, Z. Chen, J. Liao, X. Song, X. Liang, Y. Wang, J. Dong, C. V. Singh, D. Wang, Y. Li, F. D. Toste and J. Zhao, *J. Am. Chem. Soc.*, 2024, **146**, 10847–10856.
98 Y. Xiong, J. Dong, Z. Q. Huang, P. Xin, W. Chen, Y. Wang, Z. Li, Z. Jin, W. Xing, Z. Zhuang, J. Ye, X. Wei, R. Cao, L. Gu, S. Shun, L. Zhuang, X. Chen, H. Yang, C. Chen, Q. Peng, C. R. Chang, D. Wang and Y. Li, *Nat. Nanotechnol.*, 2020, **15**, 390–397.
99 Y. Hu, C. Chen, T. Shen, X. Guo, C. Yang, D. Wang and Y. Zhu, *Adv. Sci.*, 2022, **9**, 2205299.
100 Y. Chen, H. Zhu, X. Ding, H. Wang, W. Qiu, J. Song and S. Pang, *ACS Appl. Nano Mater.*, 2024, **7**, 8063–8073.
101 Q. Feng, S. Zhao, Q. Xu, W. Chen, S. Tian, Y. Wang, W. Yan, J. Luo, D. Wang and Y. Li, *Adv. Mater.*, 2019, **31**, 1901024.
102 S. Wei, X. Liu, C. Wang, X. Liu, Q. Zhang and Z. Li, *ACS Nano*, 2023, **17**, 14831–14839.
103 M. Kwak, J. Bok, B. H. Lee, J. Kim, Y. Seo, S. Kim, H. Choi, W. Ko, W. H. Antink, C. W. Lee, G. H. Yim, H. Seung, C. Park, K. S. Lee, D. H. Kim, T. Hyeon and D. Yoo, *Chem. Sci.*, 2022, **13**, 8536–8542.
104 E. Zhao, L. Chen, Q. Zhu, Z. Chen, Y. Wei, W. Zhang, L. Dong, W. Fang and Z. Chen, *Chin. J. Chem.*, 2023, **41**, 3281–3289.
105 X. Li, A. E. Surkus, J. Rabeah, M. Anwar, S. Dastigir, H. Junge, A. Brückner and M. Beller, *Angew. Chem., Int. Ed.*, 2020, **59**, 15849–15854.
106 Z. Li, Y. Chen, X. Lu, H. Li, L. Leng, T. Zhang and J. H. Horton, *Nano Res.*, 2022, **15**, 4023–4031.
107 Y. Xiong, W. Sun, Y. Han, P. Xin, X. Zheng, W. Yan, J. Dong, J. Zhang, D. Wang and Y. Li, *Nano Res.*, 2021, **14**, 2418–2423.
108 J. Liang, Q. Song, J. Wu, Q. Lei, J. Li, W. Zhang, Z. Huang, T. Kang, H. Xu, P. Wang, X. Zhou, P. K. Wong, H. Li, X. Meng, Z. Jiang and C. S. Lee, *ACS Nano*, 2022, **16**, 4152–4161.
109 L. Duan, C. T. Hung, J. Wang, C. Wang, B. Ma, W. Zhang, Y. Ma, Z. Zhao, C. Yang, T. Zhao, L. Peng, D. Liu, D. Zhao and W. Li, *Angew. Chem.*, 2022, **134**, e202211307.
110 Y. Lu, Z. Zhang, H. Wang and Y. Wang, *Appl. Catal., B*, 2021, **292**, 120162.
111 Z. Chen, E. Vorobyeva, S. Mitchell, E. Fako, M. A. Ortuño, N. López, S. M. Colins, P. A. Midgley, S. Richard, G. Vilé and J. Pérez-Ramírez, *Nat. Nanotechnol.*, 2018, **13**, 702–707.
112 T. Yu, L. Tao, Z. Liu, X. Zhang, T. Gan, W. Yan, L. Zheng, G. Meng, W. Chen, S. Liu, C. Ye and J. Zhang, *ACS Appl. Mater. Interfaces*, 2024, **16**, 20391–20399.
113 Z. Chen, J. Liu, M. J. Koh and K. P. Loh, *Adv. Mater.*, 2022, **34**, 2103882.
114 D. Ding, J. Wang, J. Xi, X. Liu, G. Lu and Y. Wang, *Green Chem.*, 2014, **16**, 3846–3853.
115 J. C. Serrano-Ruiz, R. Luque and A. Sepú lveda-Escribano, *Chem. Soc. Rev.*, 2011, **40**, 5266–5281.
116 D. M. Alonso, S. G. Wettstein and J. A. Dumesic, *Green Chem.*, 2013, **15**, 584–595.
117 S. Shao, Y. Yang, K. Sun, S. Yang, A. Li, F. Yang, X. Luo, S. Hao and Y. Ke, *ACS Catal.*, 2021, **11**, 12146–12158.
118 L. Lin, X. Han, B. Han and S. Yang, *Chem. Soc. Rev.*, 2021, **50**, 11270–11292.
119 T. Cui, L. Ma, S. Wang, C. Ye, X. Liang, Z. Zhang, G. Meng, L. Zheng, H. S. Hu, J. Zhang, H. Duan, D. Wang and Y. Li, *J. Am. Chem. Soc.*, 2021, **143**, 9429–9439.
120 W. Gu, A. Pei, S. Zhang, F. Jiang, Y. Jia, Q. Qin, R. Du, Z. Li, R. Liu, Y. Qiu, K. Yan, Y. Zhao, C. Liang and G. Chen, *ACS Appl. Mater. Interfaces*, 2023, **15**, 28036–28043.
121 Z. Zhang, J. Liu, J. Wang, Q. Wang, Y. Wang, K. Wang, Z. Wang, M. Gu, Z. Tang, J. Lim, T. Zhao and F. Ciucci, *Nat. Commun.*, 2021, **12**, 5235.
122 M. D. Marcinkowski, M. T. Darby, J. Liu, J. M. Wimble, F. R. Lucci, S. Lee, A. Michaelides, M. Flytzani-Stephanopoulos, M. Stamatakis and E. C. H. Sykes, *Nat. Chem.*, 2018, **10**, 325–332.
123 H. Guo, J. Zhao, Y. Chen, X. Lu, Y. Yang, C. Ding, L. Wu, L. Tan, J. Long, G. Yang, Y. Tang, N. Tsubaki and X. Gu, *ACS Catal.*, 2024, **14**, 703–717.
124 Y. Lu, T. Liu, C. L. Dong, Y. C. Huang, Y. Li, J. Chen, Y. Zou and S. Wang, *Adv. Mater.*, 2021, **33**, 2007056.
125 Y. Shao, Q. Xia, L. Dong, X. Liu, X. Han, S. F. Parker, Y. Cheng, L. L. Daemen, A. J. Ramirez-Cuesta, S. Yang and Y. Wang, *Nat. Commun.*, 2017, **8**, 16104.
126 S. Tian, W. Gong, W. Chen, N. Lin, Y. Zhu, Q. Feng, Q. Xu, Q. Fu, C. Chen, J. Luo, W. Yan, H. Zhao, D. Wang and Y. Li, *ACS Catal.*, 2019, **9**, 5223–5230.
127 P. Sudarsanam, E. Peeters, E. V. Makshina, V. I. Parvulescu and B. F. Sels, *Chem. Soc. Rev.*, 2019, **48**, 2366–2421.

128 A. Shafiee, N. Rabiee, S. Ahmadi, M. Baneshi, M. Khatami, S. Iravani and R. S. Varma, *ACS Appl. Nano Mater.*, 2022, **5**, 55–86.
129 Y. Pan, Y. Qian, X. Zheng, S. Q. Chu, Y. Yang, C. Ding, X. Wang, S. H. Yu and H. L. Jiang, *Natl. Sci. Rev.*, 2021, **8**, nwaa224.
130 M. Zhang, Y. G. Wang, W. Chen, J. Dong, L. Zheng, J. Luo, J. Wan, S. Tian, W. C. Cheong, D. Wang and Y. Li, *J. Am. Chem. Soc.*, 2017, **139**, 10976–10979.
131 Q. Li, H. Wang, Z. Tian, Y. Weng, C. Wang, J. Ma, C. Zhu, W. Li, Q. Liu and L. Ma, *Catal. Sci. Technol.*, 2019, **9**, 1570–1580.
132 K. S. Kanakikodi, N. Kulal, K. S. Subramanya, M. S. Puneethkumar, B. B. Kulkarni, G. V. Shanbhag and S. P. Maradur, *Mol. Catal.*, 2024, **552**, 113667.
133 N. T. do Prado, T. E. Souza, A. R. T. Machado, P. P. Souza, R. S. Monteiro and L. C. Oliveira, *J. Mol. Catal. A:Chem.*, 2016, **422**, 23–34.
134 Y. Yin, Y. Qi, C. Ma, W. Li, S. Luo and S. Liu, *Fuel Process. Technol.*, 2023, **245**, 107752.
135 B. Ma, Y. Wang, X. Guo, X. Tong, C. Liu, Y. Wang and X. Guo, *Appl. Catal., A*, 2018, **552**, 70–76.
136 P. Zhu, W. Zhang, Q. Li and H. Xia, *ACS Sustain. Chem. Eng.*, 2022, **10**, 8778–8787.
137 W. Zhang, X. Li, S. Liu, J. Qiu, J. An, J. Yao, S. Zuo, B. Zhang, H. Xia and C. Li, *ChemSusChem*, 2022, **15**, e202102158.
138 L. Xiong, H. Qi, S. Zhang, L. Zhang, X. Liu, A. Wang and J. Tang, *Adv. Mater.*, 2023, **35**, 2209646.
139 J. Ma, X. Li, Y. Li, G. Jiao, H. Su, D. Xiao, S. Zhai and R. Sun, *Adv. Powder Mater.*, 2022, **1**, 100058.
140 X. Tan, S. Si, D. Xiao, X. Bao, K. Song, Z. Wang, Y. Liu, Z. Zheng, P. Wang, Y. Dai, B. Huang and H. Cheng, *ACS Catal.*, 2023, **13**, 14395–14403.
141 Y. Lou, Y. Zheng, X. Li, N. Ta, J. Xu, Y. Nie, K. Cho and J. Liu, *J. Am. Chem. Soc.*, 2019, **141**, 19289–19295.
142 L. Zhang, M. Zhou, A. Wang and T. Zhang, *Chem. Rev.*, 2019, **120**, 683–733.
143 X. Lan and T. Wang, *ACS Catal.*, 2020, **10**, 2764–2790.
144 Z. Chen, J. Liu, M. J. Koh and K. P. Loh, *Adv. Mater.*, 2022, **34**, 2103882.
145 D. M. Alonso, S. G. Wettstein and J. A. Dumesic, *Chem. Soc. Rev.*, 2012, **41**, 8075–8098.
146 J. F. Yang, S. S. Li, L. L. Zhang, X. Y. Liu, J. H. Wang, X. L. Pan, N. Li, A. Q. Wang, Y. Cong, X. D. Wang and T. Zhang, *Appl. Catal., B*, 2017, **201**, 266–277.
147 F. Huang, Y. Deng, Y. Chen, X. Cai, M. Peng, Z. Jia, J. Xie, D. Xiao, X. Wen, N. Wang, Z. Jiang, H. Liu and D. Ma, *Nat. Commun.*, 2019, **10**, 4431.
148 X. Huang, Y. Xia, Y. Cao, X. Zheng, H. Pan, J. Zhu, C. Ma, H. Wang, J. Li, R. You, S. Wei, W. Huang and J. Lu, *Nano Res.*, 2017, **10**, 1302–1312.
149 X. Gong, D. C. Li, Q. Zhang, W. Wang, Z. Tian, G. Su, M. Huang and G. H. Wang, *Nano Res.*, 2023, **16**, 11358–11365.
150 L. Xiong and J. Tang, *Adv. Energy Mater.*, 2021, **11**, 2003216.
151 J. C. Védrine, *ChemSusChem*, 2019, **12**, 577–588.
152 S. Zhao, Y. Wen, X. Liu, X. Pen, F. Lü, F. Gao, X. Xie, C. Du, H. Yi, D. Kang and X. Tang, *Nano Res.*, 2020, **13**, 1544–1551.
153 Y. Pan, Y. Chen, K. Wu, Z. Chen, S. Liu, X. Cao, W. C. Cheong, T. Meng, J. Luo, L. Zheng, C. Liu, D. Wang, Q. Peng, J. Li and C. Chen, *Nat. Commun.*, 2019, **10**, 4290.
154 R. Fan, J. Lu, H. Yan, Y. Liu, X. Zhou, H. Zhao, X. Feng, X. Chen and C. Yang, *Front. Chem. Sci. Eng.*, 2024, **18**, 137.
155 T. Zhang, Z. Sun, S. Li, B. Wang, Y. Liu, R. Zhang and Z. Zhao, *Nat. Commun.*, 2022, **13**, 6996.
156 W. Chen, H. Jin, F. He, P. Cui, C. Cao and W. Song, *Nano Res.*, 2021, **15**, 1–9.
157 G. Ding, L. Hao, H. Xu, L. Wang, J. Chen, T. Li, X. Tu and Q. Zhang, *Commun. Chem.*, 2020, **3**, 43.
158 M. C. D'Alterio, È. Casals-Cruañas, N. V. Tzouras, G. Talarico, S. P. Nolan and A. Poater, *Chem.–Eur. J.*, 2021, **27**, 13481–13493.
159 J. Liu, Z. Chen, C. Liu, B. Zhang, Y. Du, C. F. Liu, L. Ma, S. Xi, R. Li, X. Zhao, J. Song, X. Z. Sui, W. Yu, L. Miao, J. Jiang, M. J. Koh and K. P. Loh, *J. Mater. Chem.*, 2021, **9**, 11427–11432.
160 J. Du, Y. Peng, X. Guo, G. Zhang, F. Zhang, X. Fan, W. Peng and Y. Li, *Catalysts*, 2023, **13**, 651.
161 S. Ji, X. Lu, M. Zhang, L. Leng, H. Liu, K. Yin, C. Xu, C. He, J. H. Horton, J. Zhang and Z. Li, *Chem. Eng. J.*, 2023, **452**, 139205.
162 A. Vice, N. Langer, B. Reinhart and O. Kedem, *Inorg. Chem.*, 2023, **62**, 21479–21486.
163 G. Zakem and P. Christopher, *ACS Catal.*, 2023, **13**, 5502–5515.
164 A. H. Jenkins, E. E. Dunphy, M. F. Toney, C. B. Musgrave and J. W. Medlin, *ACS Catal.*, 2023, **13**, 15340–15350.
165 X. Jia, J. Zhao, W. Zhang, X. Fu, J. Long, Q. Gu and Z. Gao, *ChemistrySelect*, 2022, **7**, e202202973.
166 Y. Xu, Y. Li, Y. Wei, H. Liang, T. Xu, Y. Sun and J. Bai, *Colloids Surf., A*, 2024, **690**, 133751.
167 S. Huang, Y. Chang, Z. Li, J. Cao, Y. Song, J. Gao, L. Sun and J. Hou, *Adv. Funct. Mater.*, 2023, **33**, 2211631.
168 C. Han, R. Qi, R. Sun, K. Fan, B. Johannessen, D. C. Qi, S. Cao and J. Xu, *Appl. Catal., B*, 2023, **320**, 121954.
169 Q. Xiao, S. Sarina, E. Jaatinen, J. Jia, D. P. Arnold, H. Liu and H. Zhu, *Green Chem.*, 2014, **16**, 4272–4285.
170 D. F. Akl, D. Poier, S. C. D'Angelo, T. P. Araújo, V. Tulus, O. V. Safonova, S. Mitchell, G. Guillén-Gosálbez and J. Pérez-Ramírez, *Green Chem.*, 2022, **24**, 6879–6888.
171 N. Wang, L. Ma, J. Wang, Y. Zhang and R. Jiang, *ChemPlusChem*, 2019, **84**, 1164–1168.
172 L. Zhang, A. Wang, J. T. Miller, X. Liu, X. Yang, W. Wang, L. Li, Y. Huang, C. Y. Mou and T. Zhang, *ACS Catal.*, 2014, **4**, 1546–1553.
173 S. Mukherjee, A. Das, A. K. Das, A. Sheriff, K. Sunny, A. S. Nair, S. Bhandary, R. Bhowal, D. Chopra, B. Pathak, S. Yamajoe and S. Mandal, *Chem. Mater.*, 2023, **35**, 1659–1666.
174 X. Zhang, Z. Sun, B. Wang, Y. Tang, L. Nguyen, Y. Li and F. F. Tao, *J. Am. Chem. Soc.*, 2018, **140**, 954–962.

175 B. Wu, T. Lin, R. Yang, M. Huang, H. Zhang, J. Li, F. Sun, F. Song, Z. Jiang, L. Zhong and Y. Sun, *Green Chem.*, 2021, **23**, 4753–4761.
176 Z. Li, X. Lu, C. Guo, S. Ji, H. Liu, C. Guo, X. Lu, C. Wang, W. Yan, B. Liu, W. Wu, J. H. Horton, S. Shin and Y. Wang, *Nat. Commun.*, 2024, **15**, 3195.
177 T. Zhang, Z. Xie, L. Jiang, W. Zhao, S. Cao, B. Wang, R. Si, R. Zhang, Y. Liu and Z. Zhao, *Chem. Eng. J.*, 2022, **443**, 136416.
178 P. Ren, Q. Li, T. Song, Z. Wang, K. Motokura and Y. Yang, *ChemCatChem*, 2021, **13**, 3960–3966.
179 G. Vilé, G. Di Liberto, S. Tosoni, A. Sivo, V. Ruta, M. Nachtegaal, A. H. Clark, S. Agnoli, Y. Zou, A. Savateev, M. Antonietti and G. Pacchioni, *ACS Catal.*, 2022, **12**, 2947–2958.
180 J. Song, Z. Chen, X. Cai, X. Zhou, G. Zhan, R. Li, P. Wei, N. Yan, S. Xi and K. P. Loh, *Adv. Mater.*, 2022, **34**, 2204638.
181 C. Wang, D. Ikhlef, S. Kahlal, J. Y. Saillard and D. Astruc, *Coord. Chem. Rev.*, 2016, **316**, 1–20.
182 J. S. Oakdale, R. K. Sit and V. V. Fokin, *Chem.–Eur. J.*, 2014, **20**, 11101–11110.
183 Y. Li, Z. Wang, T. Xia, H. Ju, K. Zhang, R. Long, Q. Xu, C. Wang, L. Song, J. Zhu, J. Jiang and Y. Xiong, *Adv. Mater.*, 2016, **28**, 6959–6965.
184 H. Yan, C. Su, J. He and W. Chen, *J. Mater. Chem. A*, 2018, **6**, 8793–8814.
185 G. Zhu, Y. Qi, F. Liu, S. Ma, G. Xiang, F. Jin, Z. Liu and W. Wang, *ChemSusChem*, 2021, **14**, 866–875.
186 I. H. Kim, J. Lim and S. O. Kim, *Acc. Mater. Res.*, 2021, **2**, 394–406.
187 Z. Wang, S. M. Xu, Y. Xu, L. Tan, X. Wang, Y. Zhao, H. Duan and Y. F. Song, *Chem. Sci.*, 2019, **10**, 378–384.
188 A. K. Agrahari, P. Bose, M. K. Jaiswal, S. Rajkhowa, A. S. Singh, S. Hotha, N. Mishra and V. K. Tiwari, *Chem. Rev.*, 2021, **121**, 7638–7956.
189 B. Kumru, J. Mendoza Mesa, M. Antonietti and M. Al-Naji, *ACS Sustain. Chem. Eng.*, 2019, **7**, 17574–17579.
190 B. Albada, J. F. Keijzer, H. Zuilhof and F. van Delft, *Chem. Rev.*, 2021, **121**, 7032–7058.